Application of nanotubes in conveying nanofluid: A bifurcation analysis with consideration of internal friction and geometrical imperfection

Ali Farajpour [a*], Mergen H. Ghayesh [a,†], Hamed Farokhi [b,††]

[a] *School of Mechanical Engineering, University of Adelaide, South Australia 5005, Australia*

[b] *Department of Mechanical and Construction Engineering, Northumbria University, Newcastle upon Tyne NE1 8ST, UK*

[*] *Corresponding author's email: ali.farajpourouderji@adelaide.edu.au*

[†] *Email: mergen.ghayesh@adelaide.edu.au*

[††] *Email: hamed.farokhi@northumbria.ac.uk*

Abstract

This article deals with developing a coupled scale-dependent model to explore the nonlinear bifurcation response of initially imperfect nanotubes conveying nanofluid flow taking into consideration the influences of nonlinear viscoelasticity. Furthermore, the influences of both centrifugal and Coriolis forces are considered. The Beskok-Karniadakis model is employed to capture the influences of slip at the interface between the imperfect viscoelastic nanotube and the nanofluid. A refined combination of nonlocal and strain gradient elasticities is employed for taking into consideration size influences. After formulating the kinetic energy, elastic energy, viscous work and external work, the nonlinear coupled equations are derived for the nanofluid-conveying nanosystem, which simultaneously vibrates along the transverse and longitudinal directions. The nonlinear dynamical characteristics are calculated via utilising a Galerkin procedure and a direct-time-integration technique. It is found that chaotic regions can be removed by imposing a proper geometric imperfection.

Keywords: Bifurcation; Scale effects; Initial imperfection; Viscoelasticity; Coupled motion

1. Introduction

In a number of nanoscale electromechanical devices, the general performance is significantly influenced by interactions between the solid structural part and the fluid. For instance, in nanofluidic devices, which have been used for various applications from cell separation to water purification [1], the interactions between the channels and the fluid affect the efficiency of the device. Developing more accurate and comprehensive continuum-based models in order to understand these interactions would help us to better design and manufacture fluid-conveying nanoscale electromechanical devices.

An appropriate continuum-based model for a fluid-conveying nanostructure should be size-dependent since the static and dynamic behaviours of nanostructures are considerably influenced by size effects [2-10]. Several size-dependent models such as nonlocal [11-16], couple stress [17-23], and strain gradient [24, 25] theories have been introduced for nanoscale structures. In the present analysis, a refined combination of the strain gradient and nonlocal models [26-28] is utilised since it has been reported that this continuum model is capable of better capturing size influences compared to the pure nonlocal model [29]. In addition to being size-dependent, an appropriate continuum-based model for a fluid-conveying structure at nanoscales should be able to incorporate the effects of slip at the interface between the solid structure and the fluid. For this purpose, the Beskok-Karniadakis model [30] is employed.

Developing size-dependent continuum models for fluid-conveying structures at nanoscales has attracted researcher's attention recently due to the wide applications of these nanosystems. Wang and Ni [31] developed a continuum model for analysing the stability and

oscillation of carbon nanotubes (CNTs) conveying nanofluid. Lee and Chang [32] analysed the free vibration of a nanofluid-conveying single-walled CNT along the transverse direction via developing a nonlocal model of elasticity. In another investigation, a continuum model was developed by Soltani et al. [33] for capturing the influences of a surrounding medium on the mechanics of nanofluid-conveying nanotubes. A continuum-based model incorporating couple stresses was also proposed by Zeighampour and Beni [34] for exploring the time-dependent deformation of fluid-conveying tubes at nanoscales. Furthermore, the influences of a temperature change on the instability response of tubes conveying nanofluid flow were examined in the literature [35]. A nonlocal model of elasticity was developed by Maraghi et al. [36] for describing scale influences on the mechanics of fluid-conveying boron nitride nanoscale tubes. The influences of a pulsating nanofluid on the instability of a single nanotube were studied by Liang and Su [37] via applying a continuum-based model. In another analysis conducted by Askari and Esmailzadeh [38], the vibrations of tubes conveying fluid flow at nanoscales were studied incorporating the effects of a temperature change as well as the influences of a nonlinear foundation. Furthermore, the nonlocal model of elasticity was used by Oveissi et al. [39] for studying the longitudinal oscillation of nanotubes conveying nanofluid flow. In another continuum-based analysis reported in Ref. [40], an analytical method was utilised for exploring the buckling of fluid-conveying tubes with large deformations at nanoscales. Li and Hu [41] utilised a combination of strain gradient and nonlocal models for investigating the wave propagation characteristics of nanotubes conveying nanofluid flow.

In practical situations, due to some factors such as the internal energy loss, geometric nonlinearity and initial deflections, which are often ignored in the theoretical modelling, the

results of the continuum-based models are different from the real ones. In the current analysis, for the first time, a coupled nonlinear scale-dependent model is developed to examine the large-amplitude chaotic response of initially imperfect nanotubes conveying nanofluid flow capturing the influences of nonlinear viscoelasticity. The effects of Coriolis forces caused by relative translations and rotations are considered. Furthermore, the influences of centrifugal forces induced by relative fluid translation and curvature are incorporated. A refined combination of nonlocal and strain gradient elasticities is used for size influences. To capture the influences of slip at the interface between the clamped-clamped nanotube and the fluid, the Beskok-Karniadakis model is employed. The nonlinear coupled equations are derived for the nanofluid-conveying nanotube with simultaneous transverse and longitudinal motions. The dynamical characteristics of the viscoelastic imperfect nanosystem are extracted via applying a Galerkin procedure and a direct-time-integration technique. The current study would be helpful in designing fluid-conveying nanoscale electromechanical devices.

2. Slip effects at the interface between nanotube and nanofluid

For macroscale fluid-conveying pipes, a common assumption is that there is no slip at pipe/fluid interface. Nonetheless, this assumption is not valid for small-scale fluid-conveying systems such as nanotubes conveying nanofluid flow. In fact, unlike the large-scale pipes conveying fluid in which the no-slip boundary condition is valid, the wall slip effect is not negligible at nanoscales since the molecular free path is considerable compared to the diameter of the nanotube. Therefore, a reliable continuum model should take into consideration the wall

slip effect. It has been indicated that neglecting wall slip effects results in overestimated critical flow velocities [42]. For small-scale systems in which the average molecular free path is comparable to the minimum size of the tube, the Knudsen number (*Kn*) is defined by

$$Kn = \frac{a_{fp}}{\ell_{ext}}, \tag{1}$$

where ℓ_{ext} and a_{fp} denote the external characteristic dimension and average molecular free path, respectively. For the nanofluid viscosity, we have [30]

$$\mu_{nf} = \frac{\mu_{nf0}}{1 + \Lambda Kn}, \tag{2}$$

in which μ_{nf} and μ_{nf0} denote the effective and bulk viscosities, respectively; also, Λ represents a constant, which is given by

$$\Lambda = \frac{2\Lambda_0}{\pi} \tan^{-1}\left[\lambda_0 \left(Kn\right)^{\lambda_1}\right], \tag{3}$$

where coefficients λ_0, λ_1 and β are, respectively, set to $\lambda_0 = 4$, $\lambda_1 = 0.4$ and $\beta = -1$. Furthermore, for the coefficient Λ_0, one can obtain

$$\Lambda_0 = \lim_{Kn \to \infty} \Lambda = \frac{64\beta}{3\pi\beta - 12\pi} = \frac{64}{15\pi}. \tag{4}$$

Let us denote the flow speed vector, nanofluid density, pressure, gradient operator and Laplacian operator by $\boldsymbol{v}$, ρ_{nf}, P, ∇ and ∇^2, respectively. The Navier–Stokes equations are given by

$$-\nabla P + \mu_{nf}\nabla^2 \boldsymbol{v} = \rho_{nf}\frac{d\boldsymbol{v}}{dt}. \tag{5}$$

Figure 1 shows an initially imperfect viscoelastic nanotube conveying nanofluid flow. It is assumed that the nanofluid flow is of a Newtonian incompressible laminar type. Using Eq. (5), the longitudinal nanofluid speed is obtained as

$$v_x = C_2 \frac{\partial P}{\partial x} r^2 + C_1 Ln(r) + C_0, \tag{6}$$

where

$$C_2 = \frac{1}{4\mu_{nf}}. \tag{7}$$

In Eq. (6), C_1 and C_0 represent the integration constants. C_1 is zero since $Ln(r)$ (refer to Eq. (6)) takes infinite values when $r \to 0$. Utilising the Beskok-Karniadakis model, the slip velocity is determined as [30]

$$(v_x)\big|_{r=R_i} = \frac{KnR_i}{(-\beta Kn + 1)} \left(1 - \frac{2}{\sigma_v}\right) \left(\frac{\partial v_x}{\partial r}\right)\Big|_{r=R_i}, \tag{8}$$

in which σ_v and R_i stand for the tangential momentum accommodation factor and tube inner radius, respectively; the former parameter is commonly set to 0.7. Using Eqs. (6)-(8), we have

$$C_0 = \left(\frac{R_i^2}{4\mu_{nf}}\right) \frac{\partial P}{\partial x} \left[\frac{2Kn}{(-\beta Kn + 1)} \left(1 - \frac{2}{\sigma_v}\right) - 1\right]. \tag{9}$$

Substituting Eqs. (7) and (9) into Eq. (6), one can write

$$v_x = \left(\frac{1}{4\mu_{nf}}\right) \frac{\partial P}{\partial x} \left\{r^2 + R_i^2 \left[\frac{2Kn}{(-\beta Kn + 1)} \left(1 - \frac{2}{\sigma_v}\right) - 1\right]\right\}. \tag{10}$$

In order to facilitate the implementation of the slip boundary condition, a velocity correction factor is defined as

$$\kappa_{nf1}=\frac{U_{sl}}{U_{nsl}}, \tag{11}$$

in which $U_{sl}=v_{ave}^{sl}$ and $U_{nsl}=v_{ave}^{nsl}$ where "*sl*", "*nsl*" and "*ave*" are abbreviations for the slip, no-slip and average, respectively. Employing Eqs. (10) and (11), one obtains the following relation for the velocity correction factor

$$\kappa_{nf1}=\left(1+\Lambda Kn\right)\left[\frac{4Kn}{\left(-\beta Kn+1\right)}\left(\frac{2}{\sigma_v}-1\right)+1\right]. \tag{12}$$

3. Initially imperfect viscoelastic nanotubes conveying nanofluid flow

Taking into account a geometrical imperfection (i.e. $w_0(x)$), the nonlinear strain of the viscoelastic nanotube is expressed as

$$\varepsilon_{xx}=\frac{1}{2}\left(\frac{\partial w}{\partial x}\right)^2+\frac{\partial u}{\partial x}+\frac{dw_0}{dx}\frac{\partial w}{\partial x}-z\frac{\partial^2 w}{\partial x^2}. \tag{13}$$

Here ε_{xx}, u and w are the strain, axial displacement and transverse displacement, respectively. Using a refined combination of nonlocal and strain gradient elasticities, the constitutive equation of the initially imperfect viscoelastic nanotubes conveying nanofluid flow is given by

$$\begin{aligned}&\left[1-\left(e_0a\right)^2\nabla^2\right]t_{xx}=\left(1-l_{sg}^2\nabla^2\right)\left(t_{xx(el)}^{cl}+t_{xx(vis)}^{cl}\right)\\&=\left(1-l_{sg}^2\nabla^2\right)\left(E\varepsilon_{xx}+\eta\frac{\partial\varepsilon_{xx}}{\partial t}\right),\end{aligned} \tag{14}$$

where

$$t_{xx} = t_{xx(el)} + t_{xx(vis)}, \quad t_{xx}^{cl} = t_{xx(el)}^{cl} + t_{xx(vis)}^{cl}, \tag{15}$$

in which t_{xx}, t_{xx}^{cl}, η, E, e_0, a and l_{sg} stand for the nonlocal total stress, classical stress, viscosity constant, Young's modulus, calibration parameter, internal characteristic length and strain gradient parameter, respectively [43, 44]. "*vis*" and "*el*" are used as abbreviations for viscoelastic and elastic, respectively. In the current formulation, the stress resultants of the viscoelastic imperfect nanotube are defined as

$$N_{xx} = \int_A t_{xx} dA, \quad M_{xx} = \int_A z t_{xx} dA, \tag{16}$$

In Eq. (16), A denotes the nanotube cross-sectional area. Employing Eqs. (13), (14) and (16), N_{xx} and M_{xx} are obtained as

$$\begin{aligned} &\left[1-\left(e_0 a\right)^2 \nabla^2\right] N_{xx} = EA\left(1-l_{sg}^2 \nabla^2\right)\left[\frac{\partial u}{\partial x} + \frac{1}{2}\left(\frac{\partial w}{\partial x}\right)^2 + \frac{\partial w}{\partial x}\frac{dw_0}{dx}\right] \\ &+\eta A\left(1-l_{sg}^2 \nabla^2\right)\left(\frac{\partial^2 u}{\partial t \partial x} + \frac{\partial w}{\partial x}\frac{\partial^2 w}{\partial t \partial x} + \frac{\partial^2 w}{\partial t \partial x}\frac{dw_0}{dx}\right), \end{aligned} \tag{17}$$

$$\left[1-\left(e_0 a\right)^2 \nabla^2\right] M_{xx} = -EI\left(1-l_{sg}^2 \nabla^2\right)\frac{\partial^2 w}{\partial x^2} - \eta I\left(1-l_{sg}^2 \nabla^2\right)\frac{\partial^3 w}{\partial t \partial x^2}, \tag{18}$$

where I is used to indicate the nanotube moment of inertia. The elastic energy of the viscoelastic nanosystem can be formulated as

$$\begin{aligned} &\delta U_{el} = \int_0^L \int_A \left(\sigma_{xx(el)} \delta\varepsilon_{xx} + \sigma_{xx(el)}^{(1)} \nabla \delta\varepsilon_{xx}\right) dA dx = \int_0^L \int_A \left(\sigma_{xx(el)} - \nabla \sigma_{xx(el)}^{(1)}\right) \delta\varepsilon_{xx} dA dx \\ &+\left[\int_A \sigma_{xx(el)}^{(1)} \delta\varepsilon_{xx} dA\right]_0^L = \int_0^L \int_A t_{xx(el)} \delta\varepsilon_{xx} dA dx + \left[\int_A \sigma_{xx(el)}^{(1)} \delta\varepsilon_{xx} dA\right]_0^L, \end{aligned} \tag{19}$$

where $\sigma_{ij(\alpha)}$ and $\sigma^{(1)}_{ij(\alpha)}$ are the zeroth- and first-order nonlocal stresses, respectively. L and U_{el} are respectively the nanotube length and elastic energy, respectively. The viscous work of the initially imperfect viscoelastic nanotube (W_{vis}) is given by

$$\begin{aligned}\delta W_{vis} &= -\int_0^L\int_A\left(\sigma_{xx(vis)}\delta\varepsilon_{xx}+\sigma^{(1)}_{xx(vis)}\nabla\delta\varepsilon_{xx}\right)dAdx = -\int_0^L\int_A\left(\sigma_{xx(vis)}-\nabla\sigma^{(1)}_{xx(vis)}\right)\delta\varepsilon_{xx}dAdx\\ &-\left[\int_A\sigma^{(1)}_{xx(vis)}\delta\varepsilon_{xx}dA\right]_0^L = -\int_0^L\int_A t_{xx(vis)}\delta\varepsilon_{xx}dAdx-\left[\int_A\sigma^{(1)}_{xx(vis)}\delta\varepsilon_{xx}dA\right]_0^L.\end{aligned} \tag{20}$$

For the stress components of the viscoelastic nanosystem, we have

$$\begin{aligned}&t_{xx}=\sigma_{xx}-\nabla\sigma^{(1)}_{xx},\\ &t_{xx(el)}=\sigma_{xx(el)}-\nabla\sigma^{(1)}_{xx(el)},\\ &t_{xx(vis)}=\sigma_{xx(vis)}-\nabla\sigma^{(1)}_{xx(vis)},\end{aligned} \tag{21}$$

and

$$\begin{aligned}&t_{xx}=t_{xx(el)}+t_{xx(vis)},\\ &\sigma_{xx}=\sigma_{xx(el)}+\sigma_{xx(vis)},\\ &\sigma^{(1)}_{xx}=\sigma^{(1)}_{xx(el)}+\sigma^{(1)}_{xx(vis)}.\end{aligned} \tag{22}$$

For the kinetic energy of the initially imperfect viscoelastic nanotube conveying nanofluid flow, one can write

$$\begin{aligned}\delta T_k &= \int_0^L\left\{m\frac{\partial u}{\partial t}\frac{\partial\delta u}{\partial t}+M\left[\frac{\partial u}{\partial t}+\kappa_{nf1}U\left(1+\frac{\partial u}{\partial x}\right)\right]\left(\frac{\partial\delta u}{\partial t}+\kappa_{nf1}U\frac{\partial\delta u}{\partial x}\right)\right\}dx\\ &+\int_0^L\left\{m\frac{\partial w}{\partial t}\delta\frac{\partial w}{\partial t}+M\left[\frac{\partial w}{\partial t}+\kappa_{nf1}U\left(\frac{\partial w}{\partial x}+\frac{dw_0}{dx}\right)\right]\left[\frac{\partial\delta w}{\partial t}+\kappa_{nf1}U\frac{\partial\delta w}{\partial x}\right]\right\}dx.\end{aligned} \tag{23}$$

Here M and U, respectively, indicate the fluid mass per length and velocity; moreover, m represents the nanotube mass per length. For the work induced by the harmonic force $F(x)\cos(\omega t)$, one obtains

$$\delta W_F = \int_0^L F(x)\cos(\omega t)\delta w \, \mathrm{d}x. \tag{24}$$

In Eq. (24), ω and F are employed to indicate the frequency and amplitude of the harmonic force, respectively. The Hamilton's principle is described as

$$\int_{t_1}^{t_2}\left(\delta T_k + \delta W_F - \delta U_{el} + \delta W_{vis}\right)\mathrm{d}t = 0. \tag{25}$$

The substitution of Eqs. (19), (20), (23) and (24) into Eq. (25) results in two coupled equations as

$$\frac{\partial N_{xx}}{\partial x} = (m+M)\frac{\partial^2 u}{\partial t^2} + 2M\kappa_{nf1}U\frac{\partial^2 u}{\partial t\partial x} + M\left(\kappa_{nf1}\right)^2 U^2\frac{\partial^2 u}{\partial x^2}, \tag{26}$$

$$\begin{aligned}&\frac{\partial^2 M_{xx}}{\partial x^2} + \frac{\partial}{\partial x}\left[N_{xx}\left(\frac{\partial w}{\partial x} + \frac{dw_0}{dx}\right)\right] + F(x)\cos(\omega t) = \\ &(m+M)\frac{\partial^2 w}{\partial t^2} + 2M\kappa_{nf1}U\frac{\partial^2 w}{\partial t\partial x} + M\left(\kappa_{nf1}\right)^2 U^2\left(\frac{\partial^2 w}{\partial x^2} + \frac{d^2 w_0}{dx^2}\right).\end{aligned} \tag{27}$$

Employing Eqs. (26) and (27) together with Eqs. (17) and (18), M_{xx} and N_{xx} are obtained as

$$\begin{aligned}N_{xx} &= EA\left(1 - l_{sg}^2\nabla^2\right)\left[\frac{\partial u}{\partial x} + \frac{1}{2}\left(\frac{\partial w}{\partial x}\right)^2 + \frac{\partial w}{\partial x}\frac{dw_0}{dx}\right] \\ &+\eta A\left(1 - l_{sg}^2\nabla^2\right)\left(\frac{\partial^2 u}{\partial t\partial x} + \frac{\partial w}{\partial x}\frac{\partial^2 w}{\partial t\partial x} + \frac{\partial^2 w}{\partial t\partial x}\frac{dw_0}{dx}\right) \\ &+\left(e_0 a\right)^2\left[(m+M)\frac{\partial^3 u}{\partial x\partial t^2} + 2M\kappa_{nf1}U\frac{\partial^3 u}{\partial t\partial x^2} + M\left(\kappa_{nf1}\right)^2 U^2\frac{\partial^3 u}{\partial x^3}\right],\end{aligned} \tag{28}$$

$$\begin{aligned}M_{xx} &= -EI\left(1 - l_{sg}^2\nabla^2\right)\frac{\partial^2 w}{\partial x^2} - \eta I\left(1 - l_{sg}^2\nabla^2\right)\frac{\partial^3 w}{\partial t\partial x^2} \\ &-\left(e_0 a\right)^2\frac{\partial}{\partial x}\left[N_{xx}\left(\frac{\partial w}{\partial x} + \frac{dw_0}{dx}\right)\right] + (m+M)\left(e_0 a\right)^2\frac{\partial^2 w}{\partial t^2} \\ &+\left(e_0 a\right)^2\left[2M\kappa_{nf1}U\frac{\partial^2 w}{\partial t\partial x} + M\left(\kappa_{nf1}\right)^2 U^2\left(\frac{\partial^2 w}{\partial x^2} + \frac{d^2 w_0}{dx^2}\right)\right] - \left(e_0 a\right)^2 F(x)\cos(\omega t).\end{aligned} \tag{29}$$

Employing Eqs. (26)-(29), and then utilising the following set of non-dimensional parameters

$$x^* = \frac{x}{L},\quad \left(w^*,u^*,w_0^*\right) = \frac{1}{d_{out}}\left(w,u,w_0\right),\quad \chi_{sg} = \frac{l_{sg}}{L},\quad \chi_{nl} = \frac{e_0 a}{L},$$

$$\Xi = \frac{AL^2}{I},\quad t^* = t\left[\frac{EI}{L^4\left(m+M\right)}\right]^{\frac{1}{2}},\quad \bar{M} = \frac{M}{M+m},\quad s = \frac{L}{d_{out}},\quad F^* = \frac{L^4 F}{d_{out} EI}, \tag{30}$$

$$\eta^* = \frac{\eta}{E}\left[\frac{EI}{L^4\left(m+M\right)}\right]^{\frac{1}{2}},\quad \omega^* = \left[\frac{L^4\left(m+M\right)}{EI}\right]^{\frac{1}{2}}\omega,\quad U^* = \left(\frac{L^2 M}{EI}\right)^{\frac{1}{2}} U,\quad \bar{\nabla}^2 = \frac{\partial^2}{\partial x^{*2}},$$

one obtains the dimensionless nonlinear coupled equations for the initially imperfect viscoelastic nanotube conveying nanofluid flow as follows

$$\begin{aligned}
&\frac{s}{\Xi}\left[\frac{\partial^2 u}{\partial t^2} + 2\kappa_{nf1}\sqrt{\bar{M}}U\frac{\partial^2 u}{\partial x \partial t} + \left(\kappa_{nf1}\right)^2 U^2 \frac{\partial^2 u}{\partial x^2}\right] \\
&-\frac{s}{\Xi}\chi_{nl}^2\frac{\partial^2}{\partial x^2}\left[\frac{\partial^2 u}{\partial t^2} + 2\kappa_{nf1}\sqrt{\bar{M}}U\frac{\partial^2 u}{\partial t \partial x} + \left(\kappa_{nf1}\right)^2 U^2 \frac{\partial^2 u}{\partial x^2}\right] \\
&-\frac{\partial}{\partial x}\left[\frac{1}{2}\left(\frac{\partial w}{\partial x}\right)^2 + s\frac{\partial u}{\partial x} + \frac{dw_0}{dx}\frac{\partial w}{\partial x}\right] \\
&+\chi_{sg}^2\frac{\partial^3}{\partial x^3}\left[\frac{1}{2}\left(\frac{\partial w}{\partial x}\right)^2 + s\frac{\partial u}{\partial x} + \frac{dw_0}{dx}\frac{\partial w}{\partial x}\right] \\
&-\eta\frac{\partial}{\partial x}\left(s\frac{\partial^2 u}{\partial x \partial t} + \frac{\partial w}{\partial x}\frac{\partial^2 w}{\partial x \partial t} + \frac{\partial^2 w}{\partial x \partial t}\frac{dw_0}{dx}\right) \\
&+\eta\chi_{sg}^2\frac{\partial^3}{\partial x^3}\left(s\frac{\partial^2 u}{\partial t \partial x} + \frac{\partial w}{\partial x}\frac{\partial^2 w}{\partial t \partial x} + \frac{\partial^2 w}{\partial t \partial x}\frac{dw_0}{dx}\right) = 0,
\end{aligned} \tag{31}$$

$$
\begin{aligned}
&\frac{\partial^2 w}{\partial t^2}+2\kappa_{nf1}\sqrt{\bar{M}}U\frac{\partial^2 w}{\partial t\partial x}+\left(\kappa_{nf1}\right)^2U^2\left(\frac{\partial^2 w}{\partial x^2}+\frac{d^2 w_0}{dx^2}\right)\\
&-\chi_{nl}^2\frac{\partial^2}{\partial x^2}\left[\frac{\partial^2 w}{\partial t^2}+2\kappa_{nf1}\sqrt{\bar{M}}U\frac{\partial^2 w}{\partial t\partial x}+\left(\kappa_{nf1}\right)^2U^2\left(\frac{\partial^2 w}{\partial x^2}+\frac{d^2 w_0}{dx^2}\right)\right]\\
&+\frac{\partial^4 w}{\partial x^4}-\chi_{sg}^2\frac{\partial^6 w}{\partial x^6}+\eta\frac{\partial^5 w}{\partial t\partial x^4}-\eta\chi_{sg}^2\frac{\partial^7 w}{\partial t\partial x^6}-F_1\cos\left(\omega t\right)\\
&-\frac{\Xi}{s^2}\frac{\partial}{\partial x}\left\{\left(\frac{\partial w}{\partial x}+\frac{dw_0}{dx}\right)\left[\frac{1}{2}\left(\frac{\partial w}{\partial x}\right)^2+s\frac{\partial u}{\partial x}+\frac{dw_0}{dx}\frac{\partial w}{\partial x}\right]\right.\\
&-\chi_{sg}^2\left(\frac{\partial w}{\partial x}+\frac{dw_0}{dx}\right)\frac{\partial^2}{\partial x^2}\left[\frac{1}{2}\left(\frac{\partial w}{\partial x}\right)^2+s\frac{\partial u}{\partial x}+\frac{dw_0}{dx}\frac{\partial w}{\partial x}\right]\\
&+\eta\left(\frac{\partial w}{\partial x}+\frac{dw_0}{dx}\right)\left(s\frac{\partial^2 u}{\partial x\partial t}+\frac{\partial w}{\partial x}\frac{\partial^2 w}{\partial x\partial t}+\frac{\partial^2 w}{\partial x\partial t}\frac{dw_0}{dx}\right)\\
&-\chi_{sg}^2\eta\left(\frac{\partial w}{\partial x}+\frac{dw_0}{dx}\right)\frac{\partial^2}{\partial x^2}\left(s\frac{\partial^2 u}{\partial t\partial x}+\frac{\partial w}{\partial x}\frac{\partial^2 w}{\partial t\partial x}+\frac{\partial^2 w}{\partial t\partial x}\frac{dw_0}{dx}\right)\\
&\left.+\frac{s}{\Xi}\chi_{nl}^2\left(\frac{\partial w}{\partial x}+\frac{dw_0}{dx}\right)\left[\frac{\partial^3 u}{\partial x\partial t^2}+2\kappa_{nf1}\sqrt{\bar{M}}U\frac{\partial^3 u}{\partial t\partial x^2}+\left(\kappa_{nf1}\right)^2U^2\frac{\partial^3 u}{\partial x^3}\right]\right\}\\
&+\frac{\Xi}{s^2}\chi_{nl}^2\frac{\partial^3}{\partial x^3}\left\{\left(\frac{\partial w}{\partial x}+\frac{dw_0}{dx}\right)\left[\frac{1}{2}\left(\frac{\partial w}{\partial x}\right)^2+s\frac{\partial u}{\partial x}+\frac{dw_0}{dx}\frac{\partial w}{\partial x}\right]\right.\\
&-\chi_{sg}^2\left(\frac{\partial w}{\partial x}+\frac{dw_0}{dx}\right)\frac{\partial^2}{\partial x^2}\left[\frac{1}{2}\left(\frac{\partial w}{\partial x}\right)^2+s\frac{\partial u}{\partial x}+\frac{dw_0}{dx}\frac{\partial w}{\partial x}\right]\\
&+\eta\left(\frac{\partial w}{\partial x}+\frac{dw_0}{dx}\right)\left(s\frac{\partial^2 u}{\partial x\partial t}+\frac{\partial w}{\partial x}\frac{\partial^2 w}{\partial x\partial t}+\frac{\partial^2 w}{\partial x\partial t}\frac{dw_0}{dx}\right)\\
&-\eta\chi_{sg}^2\left(\frac{\partial w}{\partial x}+\frac{dw_0}{dx}\right)\frac{\partial^2}{\partial x^2}\left(s\frac{\partial^2 u}{\partial t\partial x}+\frac{\partial w}{\partial x}\frac{\partial^2 w}{\partial x\partial t}+\frac{dw_0}{dx}\frac{\partial^2 w}{\partial t\partial x}\right)\\
&\left.+\frac{s}{\Xi}\chi_{nl}^2\left(\frac{\partial w}{\partial x}+\frac{dw_0}{dx}\right)\left[\frac{\partial^3 u}{\partial x\partial t^2}+2\kappa_{nf1}\sqrt{\bar{M}}U\frac{\partial^3 u}{\partial t\partial x^2}+\left(\kappa_{nf1}\right)^2U^2\frac{\partial^3 u}{\partial x^3}\right]\right\}=0.
\end{aligned}
\tag{32}
$$

In Eqs. (31) and (32), asterisk notations are dropped for the sake of simplicity. Take into account a clamped-clamped viscoelastic imperfect nanotube, as shown in Fig. 1. It is worth mentioning that the initial imperfection is in the form of the first mode shape of the nanotube (the equation of the initial imperfection is given in the following). Using Navier–Stokes' equations

and Beskok-Karniadakis assumptions, the expected pressure required to flow fluid inside the nanotube is obtained around 8.3 MPa. Utilising Galerkin's decomposition scheme [45-48], the displacements of the nanosystem are as

$$u = \sum_{k=1}^{N_x} r_k(t)\phi_k^{(u)}(x), \\ w = \sum_{k=1}^{N_z} q_k(t)\phi_k^{(w)}(x), \tag{33}$$

in which $(r_k, \phi_k^{(u)})$ and $(q_k, \varphi_k^{(w)})$ indicate the axial and transverse sets of generalised coordinates and trial functions for the initially imperfect viscoelastic nanotube, respectively. The initial imperfection is assumed as $w_0 = A_0\phi_1^{(w)}$ in which A_0 is the imperfection amplitude. The initial shape is in the form of the natural shape of the nanotube. Substituting Eq. (33) into Eqs. (31) and (32), yields

$$\frac{s}{\Xi}\int_0^1\Bigg[\sum_{k=1}^{N_x}\phi_i^{(u)}\phi_k^{(u)}\frac{d^2r_k}{dt^2}+2\kappa_{nf1}\sqrt{\bar{M}}U\sum_{k=1}^{N_x}\phi_i^{(u)}\frac{d\phi_k^{(u)}}{dx}\frac{dr_k}{dt}$$

$$+\left(\kappa_{nf1}\right)^2U^2\sum_{k=1}^{N_x}\phi_i^{(u)}\frac{d^2\phi_k^{(u)}}{dx^2}r_k\Bigg]dx-\frac{s}{\Xi}\chi_{nl}^2\int_0^1\Bigg[\sum_{k=1}^{N_x}\phi_i^{(u)}\frac{d^2\phi_k^{(u)}}{dx^2}\frac{d^2r_k}{dt^2}$$

$$+2\kappa_{nf1}\sqrt{\bar{M}}U\sum_{k=1}^{N_x}\phi_i^{(u)}\frac{d^3\phi_k^{(u)}}{dx^3}\frac{dr_k}{dt}+\left(\kappa_{nf1}\right)^2U^2\sum_{k=1}^{N_x}\phi_i^{(u)}\frac{d^4\phi_k^{(u)}}{dx^4}r_k\Bigg]dx$$

$$-\int_0^1\phi_i^{(u)}\frac{d}{dx}\Bigg[s\sum_{k=1}^{N_x}\frac{d\phi_k^{(u)}}{dx}r_k+\frac{1}{2}\sum_{j=1}^{N_z}\sum_{k=1}^{N_z}\frac{d\phi_j^{(w)}}{dx}\frac{d\phi_k^{(w)}}{dx}q_jq_k$$

$$+A_0\sum_{k=1}^{N_z}\frac{d\phi_k^{(w)}}{dx}\frac{d\phi_1^{(w)}}{dx}q_k\Bigg]dx+\chi_{sg}^2\int_0^1\phi_i^{(u)}\frac{d^3}{dx^3}\Bigg[s\sum_{k=1}^{N_x}\frac{d\phi_k^{(u)}}{dx}r_k$$

$$+\frac{1}{2}\sum_{j=1}^{N_z}\sum_{k=1}^{N_z}\frac{d\phi_j^{(w)}}{dx}\frac{d\phi_k^{(w)}}{dx}q_jq_k+A_0\sum_{k=1}^{N_z}\frac{d\phi_k^{(w)}}{dx}\frac{d\phi_1^{(w)}}{dx}q_k\Bigg]dx$$

$$-\eta\int_0^1\phi_i^{(u)}\frac{d}{dx}\Bigg(s\sum_{k=1}^{N_x}\frac{d\phi_k^{(u)}}{dx}\frac{dr_k}{dt}+\sum_{j=1}^{N_z}\sum_{k=1}^{N_z}\frac{d\phi_j^{(w)}}{dx}\frac{d\phi_k^{(w)}}{dx}q_j\frac{dq_k}{dt}$$

$$+A_0\sum_{k=1}^{N_z}\frac{d\phi_k^{(w)}}{dx}\frac{d\phi_1^{(w)}}{dx}\frac{dq_k}{dt}\Bigg)dx+\eta\chi_{sg}^2\int_0^1\phi_i^{(u)}\frac{d^3}{dx^3}\Bigg(s\sum_{k=1}^{N_x}\frac{d\phi_k^{(u)}}{dx}\frac{dr_k}{dt} \tag{34}$$

$$+\sum_{j=1}^{N_z}\sum_{k=1}^{N_z}\frac{d\phi_j^{(w)}}{dx}\frac{d\phi_k^{(w)}}{dx}q_j\frac{dq_k}{dt}+A_0\sum_{k=1}^{N_z}\frac{d\phi_k^{(w)}}{dx}\frac{d\phi_1^{(w)}}{dx}\frac{dq_k}{dt}\Bigg)dx=0,$$

$$\int_0^1\Bigg[\sum_{k=1}^{N_z}\phi_i^{(w)}\phi_k^{(w)}\frac{d^2q_k}{dt^2}+2\kappa_{nf1}\sqrt{\bar{M}}U\sum_{k=1}^{N_z}\phi_i^{(w)}\frac{d\phi_k^{(w)}}{dx}\frac{dq_k}{dt}$$

$$+\left(\kappa_{nf1}\right)^2U^2\left(\sum_{k=1}^{N_z}\phi_i^{(w)}\frac{d^2\phi_k^{(w)}}{dx^2}q_k+A_0\phi_i^{(w)}\frac{d^2\phi_1^{(w)}}{dx^2}\right)\Bigg]dx$$

$$-\chi_{nl}^2\int_0^1\Bigg[\sum_{k=1}^{N_z}\phi_i^{(w)}\frac{d^2\phi_k^{(w)}}{dx^2}\frac{d^2q_k}{dt^2}+2\kappa_{nf1}\sqrt{\bar{M}}U\sum_{k=1}^{N_z}\phi_i^{(w)}\frac{d^3\phi_k^{(w)}}{dx^3}\frac{dq_k}{dt}$$

$$+\left(\kappa_{nf1}\right)^2U^2\left(\sum_{k=1}^{N_z}\phi_i^{(w)}\frac{d^4\phi_k^{(w)}}{dx^4}q_k+A_0\phi_i^{(w)}\frac{d^4\phi_1^{(w)}}{dx^4}\right)\Bigg]dx+$$

$$\int_0^1\Bigg[\sum_{k=1}^{N_z}\phi_i^{(w)}\frac{d^4\phi_k^{(w)}}{dx^4}q_k-\chi_{sg}^2\sum_{k=1}^{N_z}\phi_i^{(w)}\frac{d^6\phi_k^{(w)}}{dx^6}q_k+\eta\sum_{k=1}^{N_z}\phi_i^{(w)}\frac{d^4\phi_k^{(w)}}{dx^4}\frac{dq_k}{dt}$$

$$-\eta\chi_{sg}^2\sum_{k=1}^{N_z}\phi_i^{(w)}\frac{d^6\phi_k^{(w)}}{dx^6}\frac{dq_k}{dt}\Bigg]dx-\int_0^1\phi_i^{(w)}F_1\cos\left(\omega t\right)dx$$

$$-\frac{\Xi}{s^2}\int_0^1\Bigg(\phi_i^{(w)}\frac{d}{dx}\Bigg\{\left(\sum_{k=1}^{N_z}\frac{d\phi_k^{(w)}}{dx}q_k+A_0\frac{d\phi_1^{(w)}}{dx}\right)\Bigg[s\sum_{k=1}^{N_x}\frac{d\phi_k^{(u)}}{dx}r_k$$

$$+\frac{1}{2}\sum_{j=1}^{N_z}\sum_{k=1}^{N_z}\frac{d\phi_j^{(w)}}{dx}\frac{d\phi_k^{(w)}}{dx}q_jq_k+A_0\sum_{k=1}^{N_z}\frac{d\phi_k^{(w)}}{dx}\frac{d\phi_1^{(w)}}{dx}q_k\Bigg]$$

$$-\chi_{sg}^2\left(\sum_{k=1}^{N_z}\frac{d\phi_k^{(w)}}{dx}q_k+A_0\frac{d\phi_1^{(w)}}{dx}\right)\frac{d^2}{dx^2}\Bigg[s\sum_{k=1}^{N_x}\frac{d\phi_k^{(u)}}{dx}r_k$$

$$+\frac{1}{2}\sum_{j=1}^{N_z}\sum_{k=1}^{N_z}\frac{d\phi_j^{(w)}}{dx}\frac{d\phi_k^{(w)}}{dx}q_jq_k+A_0\sum_{k=1}^{N_z}\frac{d\phi_k^{(w)}}{dx}\frac{d\phi_1^{(w)}}{dx}q_k\Bigg]$$

$$+\eta\left(\sum_{k=1}^{N_z}\frac{d\phi_k^{(w)}}{dx}q_k+A_0\frac{d\phi_1^{(w)}}{dx}\right)\Bigg(s\sum_{k=1}^{N_x}\frac{d\phi_k^{(u)}}{dx}\frac{dr_k}{dt}$$

$$+\sum_{j=1}^{N_z}\sum_{k=1}^{N_z}\frac{d\phi_j^{(w)}}{dx}\frac{d\phi_k^{(w)}}{dx}q_j\frac{dq_k}{dt}+A_0\sum_{k=1}^{N_z}\frac{d\phi_k^{(w)}}{dx}\frac{d\phi_1^{(w)}}{dx}\frac{dq_k}{dt}\Bigg)$$

$$-\chi_{sg}^2\eta\left(\sum_{k=1}^{N_z}\frac{d\phi_k^{(w)}}{dx}q_k+A_0\frac{d\phi_1^{(w)}}{dx}\right)\frac{d^2}{dx^2}\Bigg(s\sum_{k=1}^{N_x}\frac{d\phi_k^{(u)}}{dx}\frac{dr_k}{dt}$$

$$+\sum_{j=1}^{N_z}\sum_{k=1}^{N_z}\frac{d\phi_j^{(w)}}{dx}\frac{d\phi_k^{(w)}}{dx}q_j\frac{dq_k}{dt}+A_0\sum_{k=1}^{N_z}\frac{d\phi_k^{(w)}}{dx}\frac{d\phi_1^{(w)}}{dx}\frac{dq_k}{dt}\Bigg)$$

$$+\frac{s}{\Xi}\chi_{nl}^2\left(\sum_{k=1}^{N_z}\frac{d\phi_k^{(w)}}{dx}q_k+A_0\frac{d\phi_1^{(w)}}{dx}\right)\Bigg[\sum_{k=1}^{N_x}\frac{d\phi_k^{(u)}}{dx}\frac{d^2r_k}{dt^2}$$

$$+2\kappa_{nf1}\sqrt{\bar{M}}U\sum_{k=1}^{N_x}\frac{d^2\phi_k^{(u)}}{dx^2}\frac{dr_k}{dt}+\left(\kappa_{nf1}\right)^2U^2\sum_{k=1}^{N_x}\frac{d^3\phi_k^{(u)}}{dx^3}r_k\Bigg]\Bigg\}\Bigg)dx$$

$$+\frac{\Xi}{s^2}\chi_{nl}^2\int_0^1\Bigg(\phi_i^{(w)}\frac{d^3}{dx^3}\Bigg\{\Bigg(\sum_{k=1}^{N_z}\frac{d\phi_k^{(w)}}{dx}q_k+A_0\frac{d\phi_1^{(w)}}{dx}\Bigg)\Bigg[s\sum_{k=1}^{N_x}\frac{d\phi_k^{(u)}}{dx}r_k$$
$$+\frac{1}{2}\sum_{j=1}^{N_z}\sum_{k=1}^{N_z}\frac{d\phi_j^{(w)}}{dx}\frac{d\phi_k^{(w)}}{dx}q_jq_k+A_0\sum_{k=1}^{N_z}\frac{d\phi_k^{(w)}}{dx}\frac{d\phi_1^{(w)}}{dx}q_k\Bigg]$$
$$-\chi_{sg}^2\Bigg(\sum_{k=1}^{N_z}\frac{d\phi_k^{(w)}}{dx}q_k+A_0\frac{d\phi_1^{(w)}}{dx}\Bigg)\frac{d^2}{dx^2}\Bigg[s\sum_{k=1}^{N_x}\frac{d\phi_k^{(u)}}{dx}r_k$$
$$+\frac{1}{2}\sum_{j=1}^{N_z}\sum_{k=1}^{N_z}\frac{d\phi_j^{(w)}}{dx}\frac{d\phi_k^{(w)}}{dx}q_jq_k+A_0\sum_{k=1}^{N_z}\frac{d\phi_k^{(w)}}{dx}\frac{d\phi_1^{(w)}}{dx}q_k\Bigg]$$
$$+\eta\Bigg(\sum_{k=1}^{N_z}\frac{d\phi_k^{(w)}}{dx}q_k+A_0\frac{d\phi_1^{(w)}}{dx}\Bigg)\Bigg(s\sum_{k=1}^{N_x}\frac{d\phi_k^{(u)}}{dx}\frac{dr_k}{dt}$$
$$+\sum_{j=1}^{N_z}\sum_{k=1}^{N_z}\frac{d\phi_j^{(w)}}{dx}\frac{d\phi_k^{(w)}}{dx}q_j\frac{dq_k}{dt}+A_0\sum_{k=1}^{N_z}\frac{d\phi_k^{(w)}}{dx}\frac{d\phi_1^{(w)}}{dx}\frac{dq_k}{dt}\Bigg)$$
$$-\chi_{sg}^2\eta\Bigg(\sum_{k=1}^{N_z}\frac{d\phi_k^{(w)}}{dx}q_k+A_0\frac{d\phi_1^{(w)}}{dx}\Bigg)\frac{d^2}{dx^2}\Bigg(s\sum_{k=1}^{N_x}\frac{d\phi_k^{(u)}}{dx}\frac{dr_k}{dt}$$
$$+\sum_{j=1}^{N_z}\sum_{k=1}^{N_z}\frac{d\phi_j^{(w)}}{dx}\frac{d\phi_k^{(w)}}{dx}q_j\frac{dq_k}{dt}+A_0\sum_{k=1}^{N_z}\frac{d\phi_k^{(w)}}{dx}\frac{d\phi_1^{(w)}}{dx}\frac{dq_k}{dt}\Bigg)$$
$$+\frac{s}{\Xi}\chi_{nl}^2\Bigg(\sum_{k=1}^{N_z}\frac{d\phi_k^{(w)}}{dx}q_k+A_0\frac{d\phi_1^{(w)}}{dx}\Bigg)\Bigg[\sum_{k=1}^{N_x}\frac{d\phi_k^{(u)}}{dx}\frac{d^2r_k}{dt^2}\qquad(35)$$
$$+2\kappa_{nf1}\sqrt{\bar{M}}U\sum_{k=1}^{N_x}\frac{d^2\phi_k^{(u)}}{dx^2}\frac{dr_k}{dt}+\left(\kappa_{nf1}\right)^2U^2\sum_{k=1}^{N_x}\frac{d^3\phi_k^{(u)}}{dx^3}r_k\Bigg]\Bigg\}\Bigg)dx=0.$$

A direct-time-integration technique is lastly utilised for developing a numerical solution for the above coupled equations.

4. Numerical results

A nanoscale tube with mass density 1024 kg/m^3, Young's modulus 610 MPa and Poisson's ratio 0.3 is taken into consideration. In addition, the outer radius, thickness and length-to-diameter ratio are assumed as R_o =290.5 nm, h=66.0 nm, L/d_o =20, respectively. The speed

correction factor and mass ratio are taken as κ_{nf1}=1.05 and $\bar{M}$=0.5915, respectively. The non-dimensional parameters of the nanotube are set to Ξ = 4006.9411, $\eta^* = 0.0003$, $\chi_{sg} = 0.05$ and $\chi_{nl} = 0.10$. Numerical calculations are performed for 20 degrees of freedom (10 degrees of freedom for each displacement component). The amplitude of the initial imperfection (dimensionless with respect to *h*) is defined as A_0. For all the cases, the forcing frequency is equal to the fundamental frequency (ω/ω_1=1.0). It should be noted that ω_1 varies when the imperfection amplitude changes.

Figure 2 is plotted in order to show the effects of imperfection amplitude on the static bifurcation diagram of the nanoscale system conveying fluid. It is found that the static bifurcation response of the nanosystem is different in the presence of a geometric imperfection. When there is no geometric imperfection, the transverse deflection suddenly changes at the critical point. However, there is no sudden change in the transverse deflection for large geometric imperfections. Figure 3 depicts the bifurcation response of perfectly straight viscoelastic tubes conveying fluid flow at nanoscales for the transverse motion at *x*=0.50 and the longitudinal motion at *x*=0.65. A set of various types of motions involving two distinct large chaotic regions (between F_1=10 and F_1=20) is observed for the perfectly straight viscoelastic nanotube.

Figure 4 illustrates the bifurcation response of initially imperfect viscoelastic tubes conveying fluid flow at nanoscales for the transverse motion at *x*=0.50 and the longitudinal motion at *x*=0.65. The imperfection amplitude is set to A_0=0.01. Comparing this figure (i.e. Fig. 4) to Fig. 3 indicates that the global dynamics of fluid-conveying viscoelastic nanotubes with a

geometric imperfection is completely different from that of perfectly straight viscoelastic nanotubes. The two chaotic regions between F_1=10 and F_1=20, which is observed in Fig. 3, can be removed by imposing a geometric imperfection. Figures 5 and 6 are plotted to provide more information about the dynamical characteristics of the nanosystem of Fig. 4 at F_1=27.0 and F_1=31.4. Initially imperfect viscoelastic tubes conveying fluid flow at nanoscales display a period-2 motion and a chaotic motion at F_1=27.0 and F_1=31.4, respectively.

Figure 7 indicates the bifurcation response of initially imperfect viscoelastic tubes conveying fluid flow at nanoscales for the transverse motion at x=0.50 and the longitudinal motion at x=0.65. The geometric imperfection is increased to A_0=0.05. It is found that the dynamical characteristics of the viscoelastic system are greatly changed by a slight increase in the imperfection amplitude. The viscoelastic nanotube displays a period-1 motion for F_1<24. Nonetheless, a period-3 region and a period-2 region are observed by further increasing F_1. For instance, Fig. 8 indicates the dynamical characteristics of the motion of the nanosystem of Fig. 7 at F_1=26.0. A period-3 motion is found for the initially imperfect viscoelastic tube conveying fluid flow at nanoscales for this loading amplitude. The bifurcation response of initially imperfect viscoelastic tubes conveying fluid flow at nanoscales for the transverse motion at x=0.50 and the longitudinal motion at x=0.65 are plotted in Fig. 9 for a higher imperfection amplitude (A_0=0.10). The nonlinear motion of the nanosystem is of period-1 for all loading amplitudes. No chaotic region is observed for the initially imperfect viscoelastic nanotube. It can be concluded that chaotic regions can be removed by imposing a proper geometric imperfection. Furthermore, Fig. 10 is plotted to provide more information about the dynamics of the periodic motion of the nanosystem of Fig. 9 at F_1=20.0.

Figure 11 gives a comparison between the bifurcation diagrams of Poincaré sections of the elastic and viscoelastic models of the initially imperfect nanotube conveying nanofluid flow. The transverse displacement predicted based on the viscoelastic model is compared with that predicted via the linear damping model. For the model of viscoelasticity, it is assumed that η=0.0003 and c_d=0 whereas η=0 and c_d=0.15 are taken into account for the linear damping model. Although for small loading amplitudes, both models yield very similar results, the bifurcation diagram of the viscoelastic model is notably different from that of the linear damping model for large loading amplitudes. Particularly, the linear damping model cannot properly predict coupled chaotic regions.

5. Conclusions

The nonlinear chaos in an initially imperfect viscoelastic nanotube conveying nanofluid flow has been analysed via utilising a refined combination of nonlocal and strain gradient elasticities. The effects of slip at the nanotube/nanofluid interface were captured employing the Beskok-Karniadakis model. The nonlinear coupled equations were derived for the initially imperfect viscoelastic nanofluid-conveying nanotube with simultaneous transverse and longitudinal motions. The nonlinear chaotic response was predicted via utilising a Galerkin scheme and a technique of direct integration. The present results indicated that nanotubes can be used to reliably convey fluid at nanoscales due to their suitable geometrical and mechanical properties. However, to avoid possible chaos in the system, an appropriate initial imperfection can be applied. For viscoelastic nanotubes with large geometric imperfections, there is no sudden change in the transverse deflection when the nanofluid velocity is increased. Furthermore, the chaotic response of initially imperfect fluid-conveying viscoelastic nanotubes is completely different from that of perfectly straight nanotubes. It was also concluded that the chaotic response of the nanofluid-conveying nanosystem is significantly changed by a slight increase in the imperfection amplitude. Chaotic regions can be eliminated by imposing an appropriate geometric imperfection. In addition, the linear damping model cannot thoroughly describe chaos in the initially imperfect fluid-conveying viscoelastic nanotube.

References

[1] J. Zhang, S. Yan, D. Yuan, G. Alici, N.-T. Nguyen, M.E. Warkiani, W. Li, Fundamentals and applications of inertial microfluidics: a review, Lab on a Chip, 16 (2016) 10-34.

[2] A. Farajpour, A. Rastgoo, Size-dependent static stability of magneto-electro-elastic CNT/MT-based composite nanoshells under external electric and magnetic fields, Microsystem Technologies, 23 (2017) 5815-5832.

[3] H. Hayati, S.A. Hosseini, O. Rahmani, Coupled twist–bending static and dynamic behavior of a curved single-walled carbon nanotube based on nonlocal theory, Microsystem Technologies, 23 (2017) 2393-2401.

[4] J. Marzbanrad, G.R. Shaghaghi, M. Boreiry, Size-dependent hygro–thermo–electro–mechanical vibration analysis of functionally graded piezoelectric nanobeams resting on Winkler–Pasternak foundation undergoing preload and magnetic field, Microsystem Technologies, 24 (2018) 1713-1731.

[5] M.Ö. Yayli, Torsional vibrations of restrained nanotubes using modified couple stress theory, Microsystem Technologies, 24 (2018) 3425-3435.

[6] F. Ebrahimi, M.R. Barati, Dynamic modeling of embedded nanoplate systems incorporating flexoelectricity and surface effects, Microsystem Technologies, (2018) 1-13.

[7] F. Ebrahimi, M.R. Barati, Damping vibration behavior of visco-elastically coupled double-layered graphene sheets based on nonlocal strain gradient theory, Microsystem Technologies, 24 (2018) 1643-1658.

[8] H. Farokhi, M.H. Ghayesh, Nonlinear thermo-mechanical behaviour of MEMS resonators, Microsystem Technologies, 23 (2017) 5303-5315.

[9] M.H. Ghayesh, A. Farajpour, Vibrations of shear deformable FG viscoelastic microbeams, Microsystem Technologies, (2018) doi: https://doi.org/10.1007/s00542-00018-04184-00548.

[10] M.H. Ghayesh, H. Farokhi, Size-dependent large-amplitude oscillations of microcantilevers, Microsystem Technologies, 23 (2017) 3477-3488.

[11] M. Aydogdu, A nonlocal rod model for axial vibration of double-walled carbon nanotubes including axial van der Waals force effects, Journal of Vibration and Control, 21 (2015) 3132-3154.

[12] M. Farajpour, A. Shahidi, F. Tabataba'i-Nasab, A. Farajpour, Vibration of initially stressed carbon nanotubes under magneto-thermal environment for nanoparticle delivery via higher-order nonlocal strain gradient theory, The European Physical Journal Plus, 133 (2018) 219.

[13] M. Aydogdu, I. Elishakoff, On the vibration of nanorods restrained by a linear spring in-span, Mechanics Research Communications, 57 (2014) 90-96.

[14] M.R. Farajpour, A. Shahidi, A. Farajpour, Resonant frequency tuning of nanobeams by piezoelectric nanowires under thermo-electro-magnetic field: a theoretical study, Micro & Nano Letters, 13 (2018) 1627-1632.

[15] S.R. Asemi, A. Farajpour, Vibration characteristics of double-piezoelectric-nanoplate-systems, IET Micro & Nano Letters, 9 (2014) 280-285.

[16] M. Farajpour, A. Shahidi, A. Farajpour, A nonlocal continuum model for the biaxial buckling analysis of composite nanoplates with shape memory alloy nanowires, Materials Research Express, 5 (2018) 035026.

[17] H. Ma, X.-L. Gao, J. Reddy, A microstructure-dependent Timoshenko beam model based on a modified couple stress theory, Journal of the Mechanics and Physics of Solids, 56 (2008) 3379-3391.

[18] H. Farokhi, M.H. Ghayesh, Size-dependent behaviour of electrically actuated microcantilever-based MEMS, International Journal of Mechanics and Materials in Design, 12 (2016) 301-315.

[19] H. Farokhi, M.H. Ghayesh, M. Amabili, Nonlinear resonant behavior of microbeams over the buckled state, Applied Physics A, 113 (2013) 297-307.

[20] M.Z. Nejad, A. Hadi, A. Farajpour, Consistent couple-stress theory for free vibration analysis of Euler-Bernoulli nano-beams made of arbitrary bi-directional functionally graded materials, Structural Engineering and Mechanics, 63 (2017) 161-169.
[21] H. Farokhi, M.H. Ghayesh, S. Hussain, Large-amplitude dynamical behaviour of microcantilevers, International Journal of Engineering Science, 106 (2016) 29-41.
[22] M.H. Ghayesh, Dynamics of functionally graded viscoelastic microbeams, International Journal of Engineering Science, 124 (2018) 115-131.
[23] H. Farokhi, M.H. Ghayesh, Nonlinear mechanics of electrically actuated microplates, International Journal of Engineering Science, 123 (2018) 197-213.
[24] B. Akgöz, Ö. Civalek, A new trigonometric beam model for buckling of strain gradient microbeams, International Journal of Mechanical Sciences, 81 (2014) 88-94.
[25] P. Malekzadeh, A.G. Shenas, S. Ziaee, Thermal buckling of functionally graded triangular microplates, Journal of the Brazilian Society of Mechanical Sciences and Engineering, 40 (2018) 418.
[26] C. Lim, G. Zhang, J. Reddy, A higher-order nonlocal elasticity and strain gradient theory and its applications in wave propagation, Journal of the Mechanics and Physics of Solids, 78 (2015) 298-313.
[27] X. Li, L. Li, Y. Hu, Z. Ding, W. Deng, Bending, buckling and vibration of axially functionally graded beams based on nonlocal strain gradient theory, Composite Structures, 165 (2017) 250-265.
[28] M.H. Ghayesh, A. Farajpour, Nonlinear mechanics of nanoscale tubes via nonlocal strain gradient theory, International Journal of Engineering Science, 129 (2018) 84-95.
[29] L. Li, Y. Hu, L. Ling, Wave propagation in viscoelastic single-walled carbon nanotubes with surface effect under magnetic field based on nonlocal strain gradient theory, Physica E: Low-dimensional Systems and Nanostructures, 75 (2016) 118-124.
[30] A. Beskok, G.E. Karniadakis, Report: a model for flows in channels, pipes, and ducts at micro and nano scales, Microscale Thermophysical Engineering, 3 (1999) 43-77.
[31] L. Wang, Q. Ni, On vibration and instability of carbon nanotubes conveying fluid, Computational Materials Science, 43 (2008) 399-402.
[32] H.-L. Lee, W.-J. Chang, Free transverse vibration of the fluid-conveying single-walled carbon nanotube using nonlocal elastic theory, Journal of Applied Physics, 103 (2008) 024302.
[33] P. Soltani, M. Taherian, A. Farshidianfar, Vibration and instability of a viscous-fluid-conveying single-walled carbon nanotube embedded in a visco-elastic medium, Journal of Physics D: Applied Physics, 43 (2010) 425401.
[34] H. Zeighampour, Y.T. Beni, Size-dependent vibration of fluid-conveying double-walled carbon nanotubes using couple stress shell theory, Physica E: Low-dimensional Systems and Nanostructures, 61 (2014) 28-39.
[35] Y.-X. Zhen, B. Fang, Y. Tang, Thermal–mechanical vibration and instability analysis of fluid-conveying double walled carbon nanotubes embedded in visco-elastic medium, Physica E: Low-dimensional Systems and Nanostructures, 44 (2011) 379-385.
[36] Z.K. Maraghi, A.G. Arani, R. Kolahchi, S. Amir, M. Bagheri, Nonlocal vibration and instability of embedded DWBNNT conveying viscose fluid, Composites Part B: Engineering, 45 (2013) 423-432.
[37] F. Liang, Y. Su, Stability analysis of a single-walled carbon nanotube conveying pulsating and viscous fluid with nonlocal effect, Applied Mathematical Modelling, 37 (2013) 6821-6828.
[38] H. Askari, E. Esmailzadeh, Forced vibration of fluid conveying carbon nanotubes considering thermal effect and nonlinear foundations, Composites Part B: Engineering, 113 (2017) 31-43.
[39] S. Oveissi, D. Toghraie, S.A. Eftekhari, Longitudinal vibration and stability analysis of carbon nanotubes conveying viscous fluid, Physica E: Low-dimensional Systems and Nanostructures, 83 (2016) 275-283.

[40] A. Ghasemi, M. Dardel, M.H. Ghasemi, M.M. Barzegari, Analytical analysis of buckling and post-buckling of fluid conveying multi-walled carbon nanotubes, Applied Mathematical Modelling, 37 (2013) 4972-4992.
[41] L. Li, Y. Hu, Wave propagation in fluid-conveying viscoelastic carbon nanotubes based on nonlocal strain gradient theory, Computational materials science, 112 (2016) 282-288.
[42] V. Rashidi, H.R. Mirdamadi, E. Shirani, A novel model for vibrations of nanotubes conveying nanoflow, Computational Materials Science, 51 (2012) 347-352.
[43] M.H. Ghayesh, A. Farajpour, A review on the mechanics of functionally graded nanoscale and microscale structures, International Journal of Engineering Science, 137 (2019) 8-36.
[44] A. Farajpour, M.H. Ghayesh, H. Farokhi, A review on the mechanics of nanostructures, International Journal of Engineering Science, 133 (2018) 231-263.
[45] H. Farokhi, M.H. Ghayesh, A. Gholipour, S. Hussain, Resonant responses of three-layered shear-deformable microbeams, Microsystem Technologies, 24 (2018) 2123-2136.
[46] H. Farokhi, M.H. Ghayesh, A. Gholipour, M. Tavallaeinejad, Stability and nonlinear dynamical analysis of functionally graded microplates, Microsystem Technologies, 24 (2018) 2109-2121.
[47] M.H. Ghayesh, Mechanics of tapered AFG shear-deformable microbeams, Microsystem Technologies, 24 (2018) 1743-1754.
[48] K. Rashvand, G. Rezazadeh, H. Mobki, M.H. Ghayesh, On the size-dependent behavior of a capacitive circular micro-plate considering the variable length-scale parameter, International Journal of Mechanical Sciences, 77 (2013) 333-342.

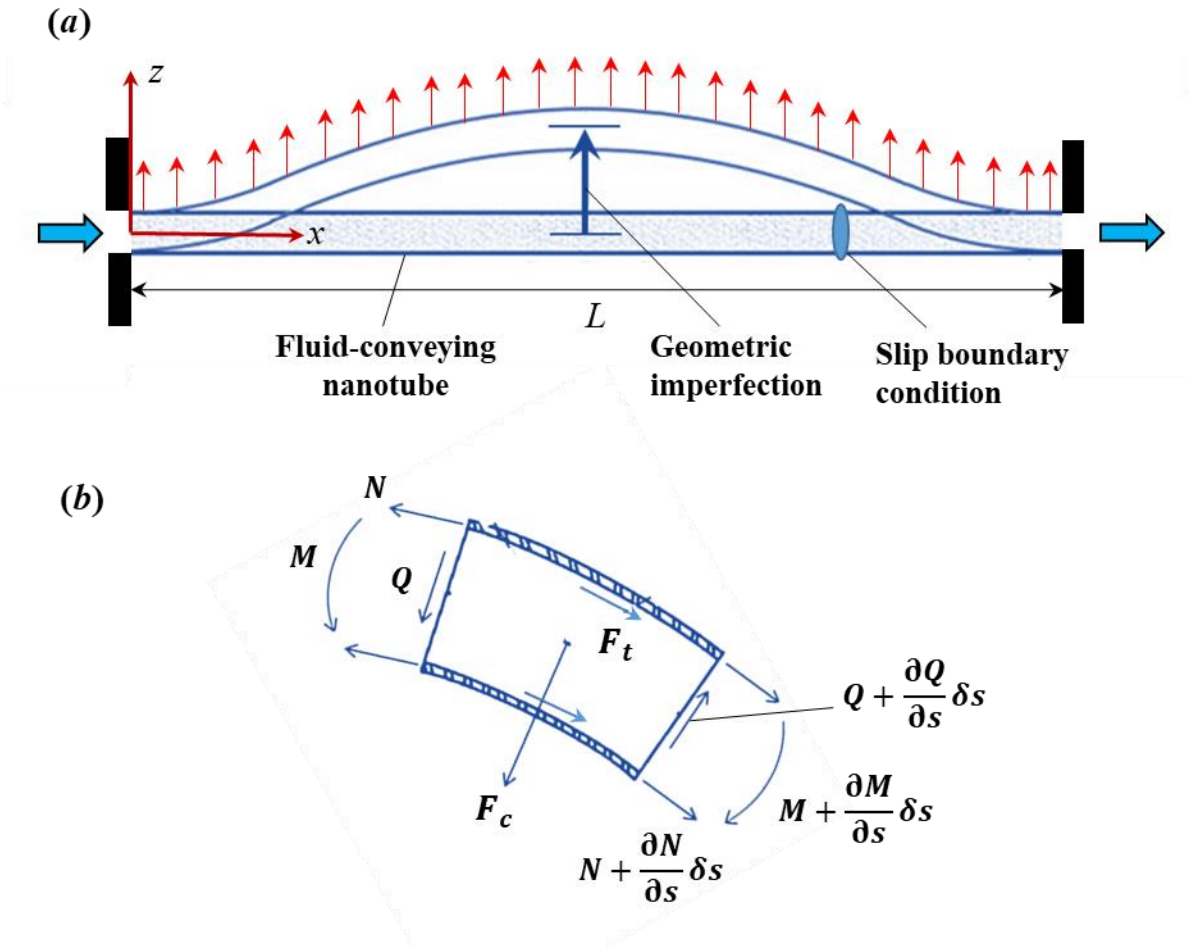

Figure 1: (a) An initially imperfect viscoelastic nanotube conveying nanofluid flow, and (b) forces exerted on an element of the nanotube.

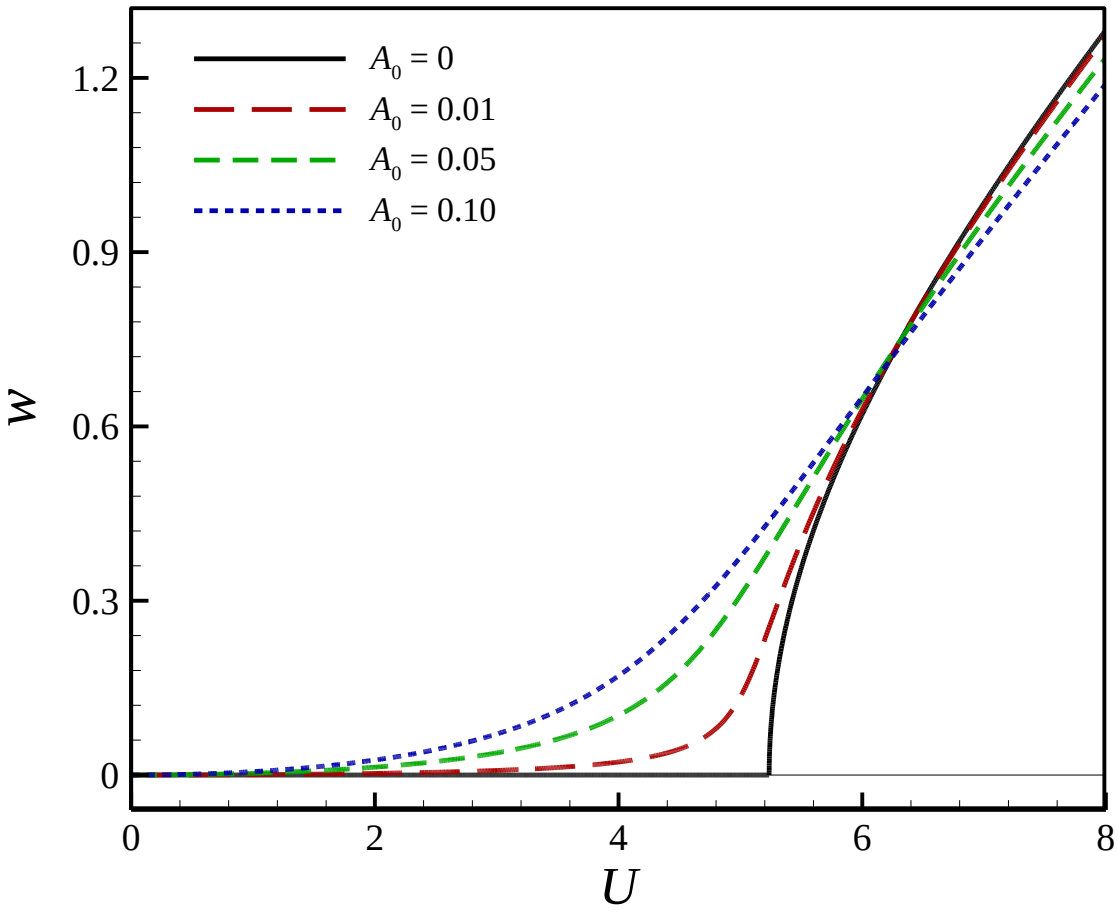

Figure 2: Imperfection effects on the static bifurcation diagram of the nanosystem. Thin solid line denotes unstable solution.

(a)

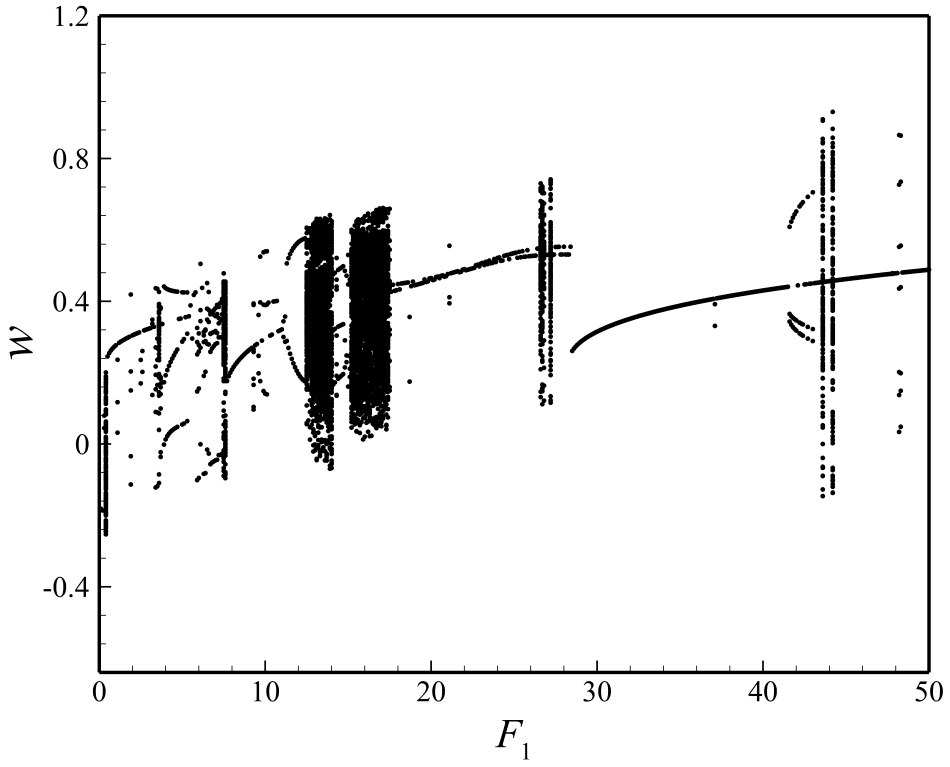

(b)

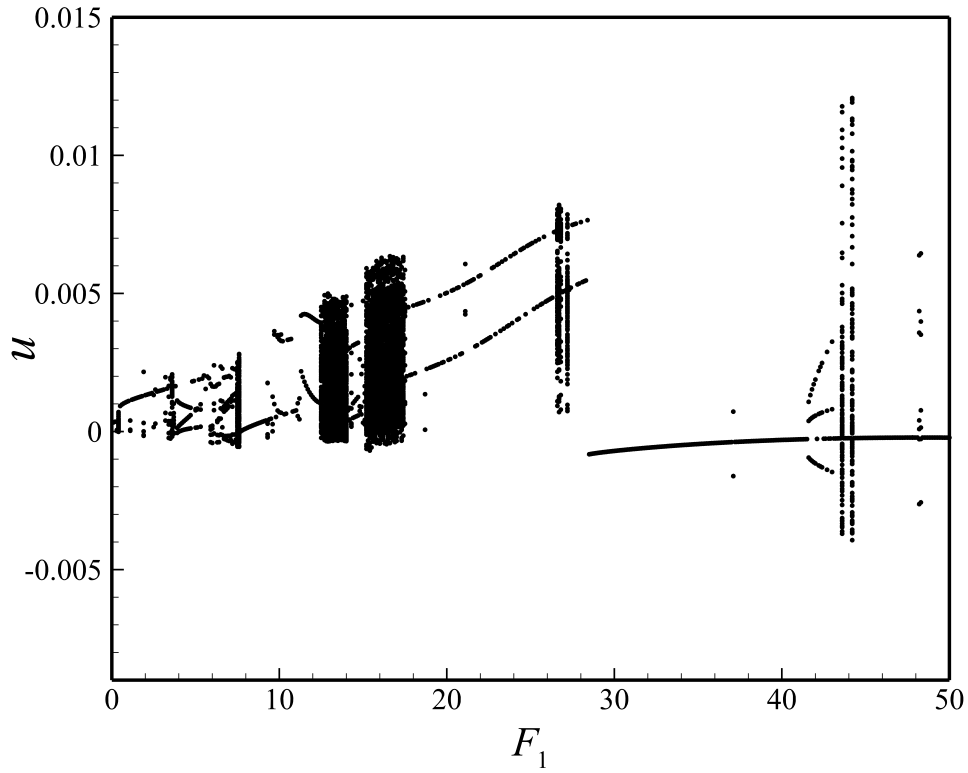

Figure 3: Bifurcation response of the perfectly straight viscoelastic tube conveying fluid flow at nanoscales: (a) *w* at *x*=0.50; (b) *u* at *x*=0.65 (U = 5.28, A_0=0, ω_1= 2.9347, and ω/ω_1=1.0).

(a)

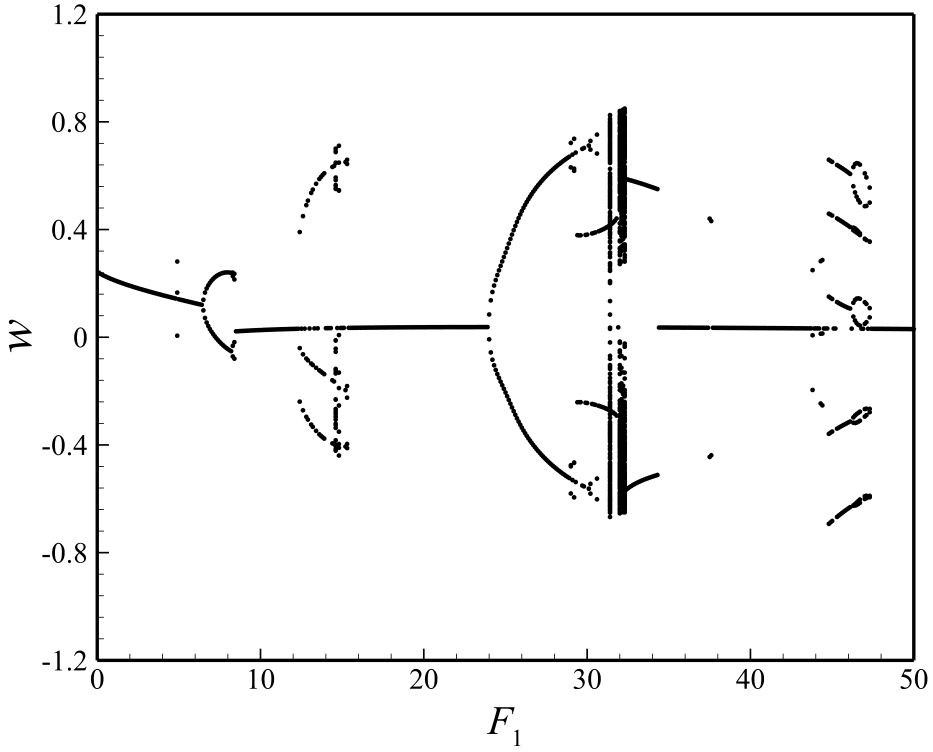

(b)

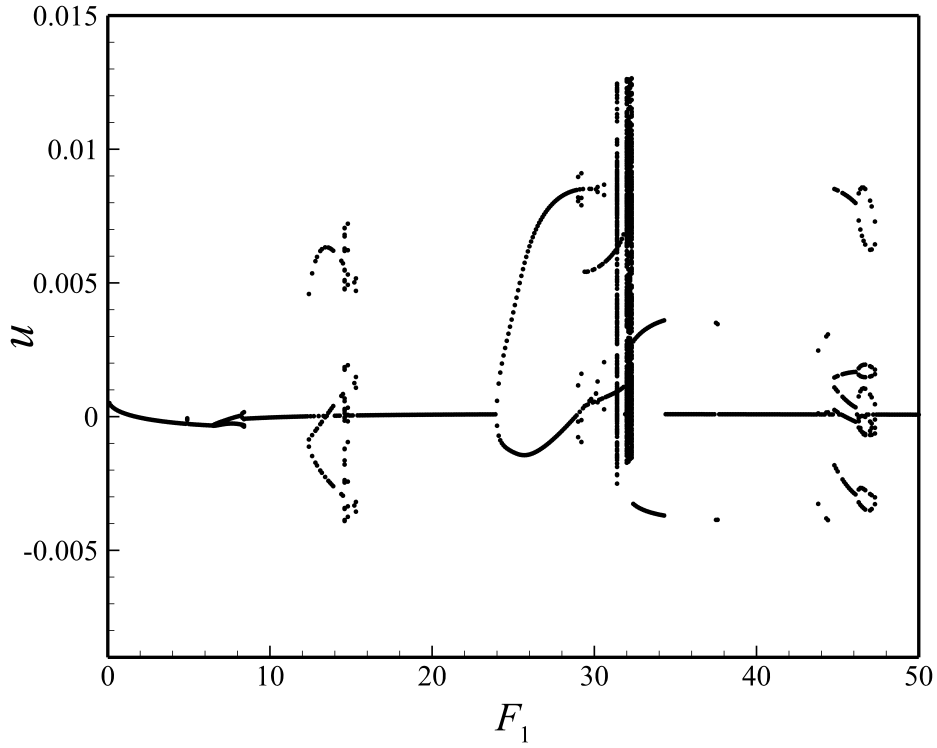

Figure 4: Bifurcation response of the initially imperfect viscoelastic tube conveying fluid flow at nanoscales: (a) *w* at *x*=0.50; (b) *u* at *x*=0.65 (*U* = 5.28, A_0=0.01, ω_1= 7.1609, and ω/ω_1=1.0).

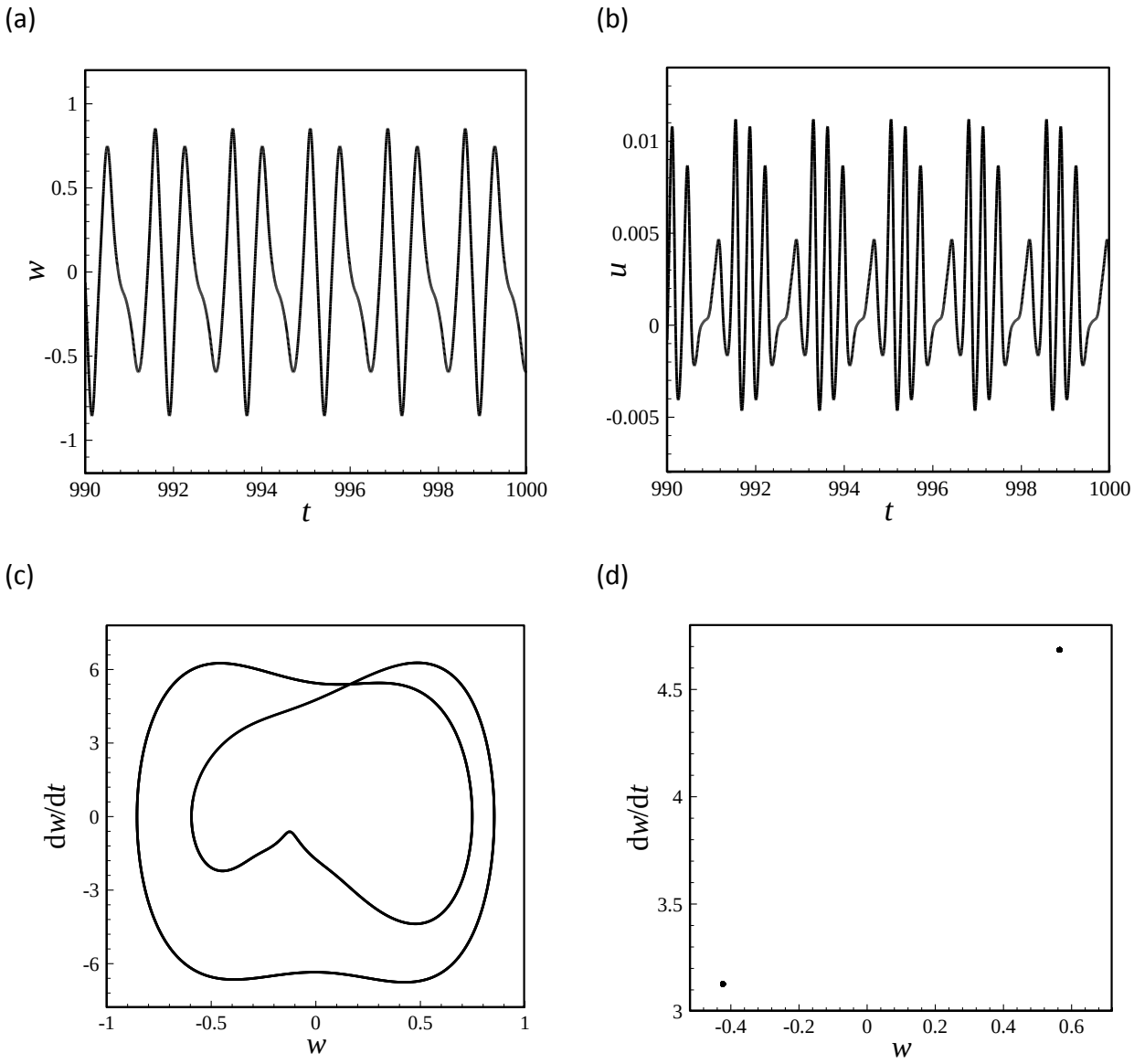

Figure 5: Dynamics of the nanosystem of Fig. 4 at F_1=27.0: (a, b) time histories of w (at x=0.5) and u (at x=0.65), respectively; (c, d) phase-plane portrait and Poincaré section of w (at x=0.5), respectively.

(a)

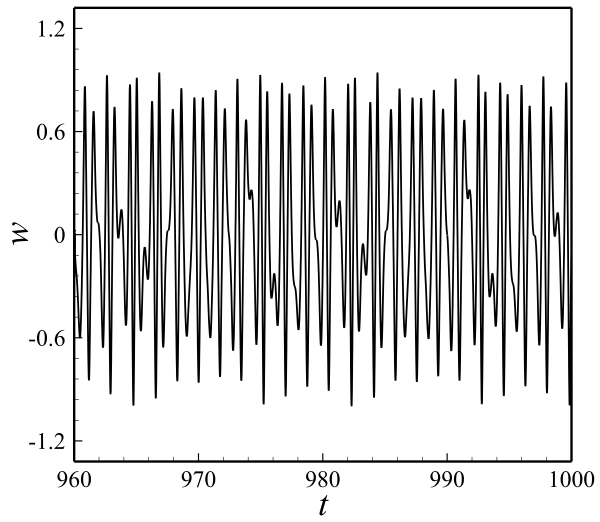
1.2
0.6
0
-0.6
-1.2
w
960
970
980
990
1000
t

(b)

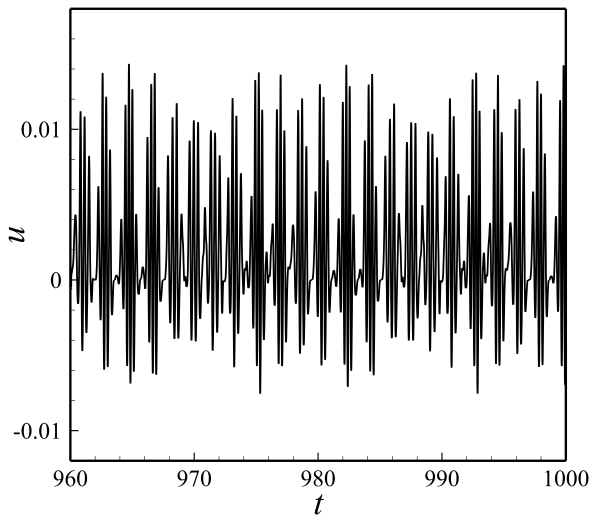
0.01
0
-0.01
u
960
970
980
990
1000
t

(c)

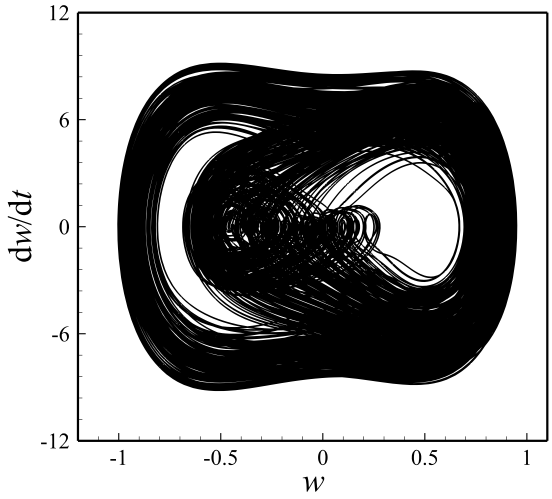
12
6
0
-6
-12
dw/dt
-1
-0.5
0
0.5
1
w

(d)

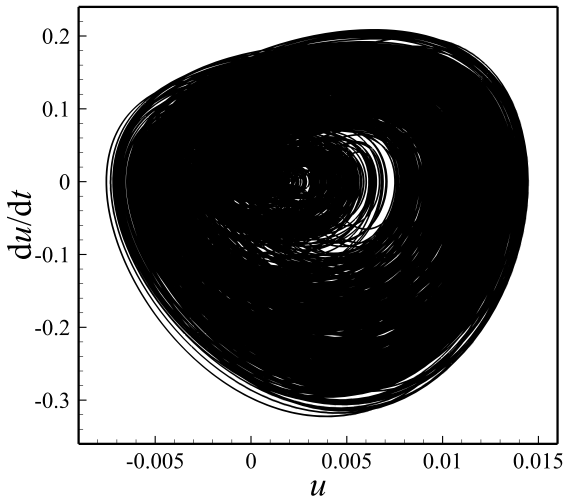
0.2
0.1
0
-0.1
-0.2
-0.3
du/dt
-0.005
0
0.005
0.01
0.015
u

(e) (f)

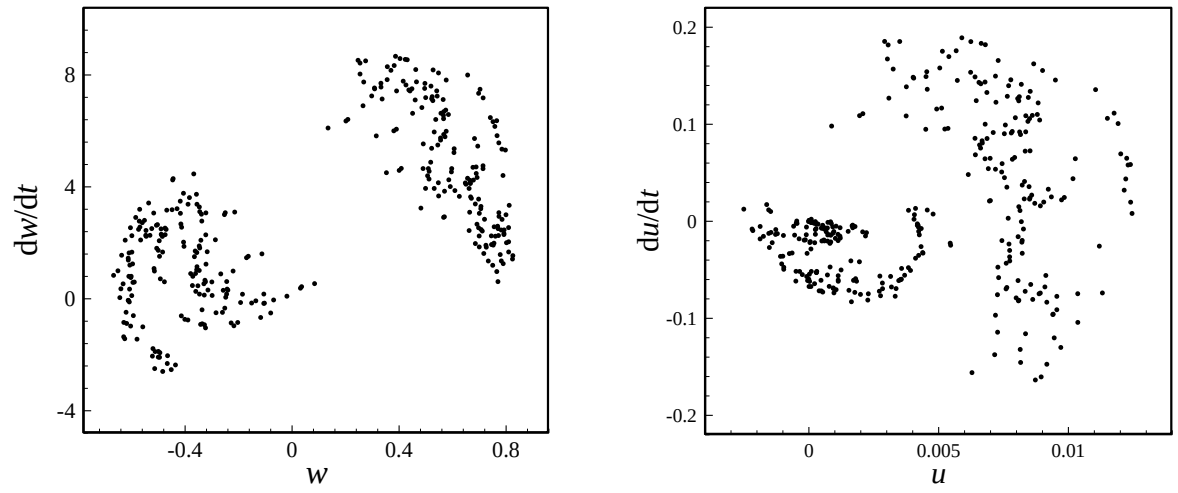

Figure 6: Dynamics of the nanosystem of Fig. 4 at F_1=31.4: (a, b) time histories of *w* (at *x*=0.5) and *u* (at *x*=0.65), respectively; (c, d) phase-plane portraits of *w* (at *x*=0.5) and *u* (at *x*=0.65), respectively; (e) Poincaré sections of *w* (at *x*=0.5) and *u* (at *x*=0.65), respectively.

(a)

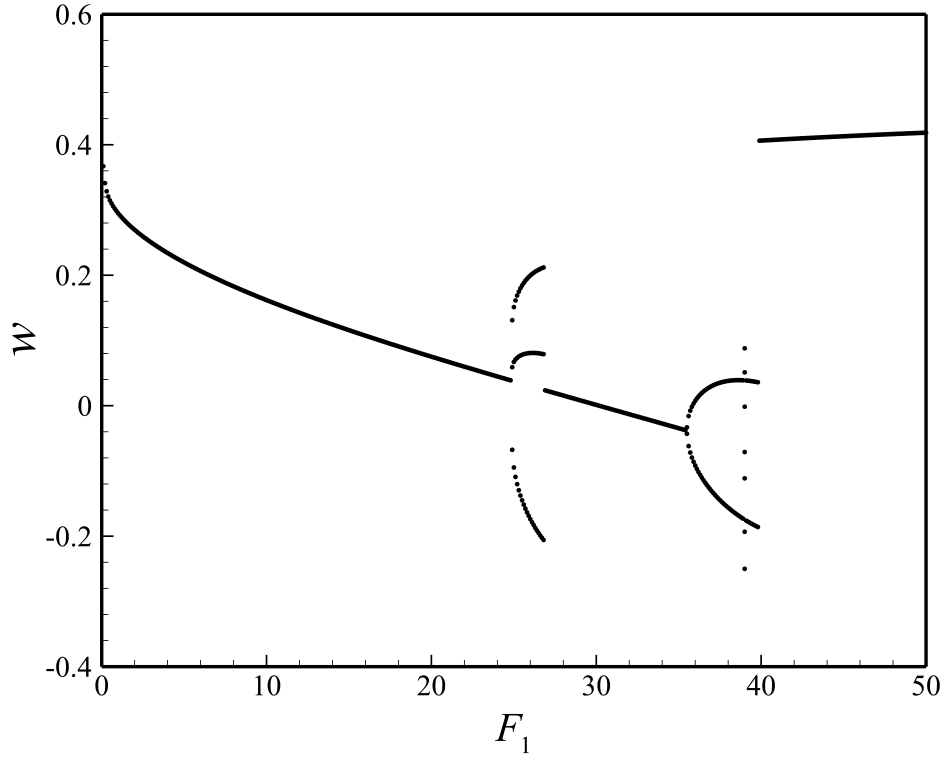

(b)

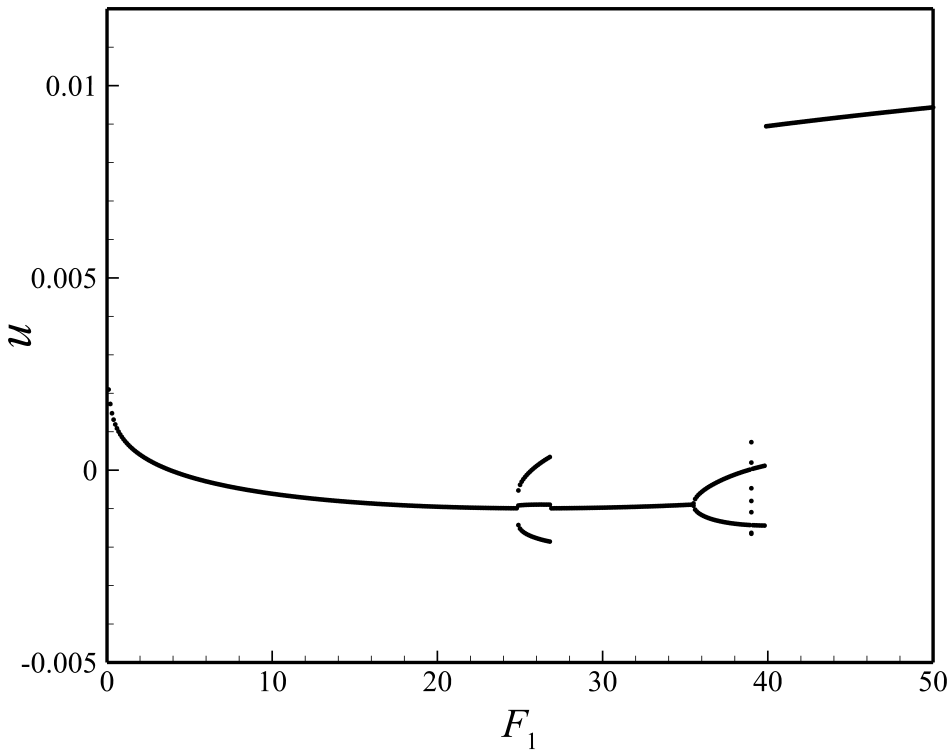

Figure 7: Bifurcation response of the initially imperfect viscoelastic tube conveying fluid flow at nanoscales: (a) *w* at *x*=0.50; (b) *u* at *x*=0.65 (U = 5.28, A_0=0.05, ω_1= 12.1073, and ω/ω_1=1.0).

(a)

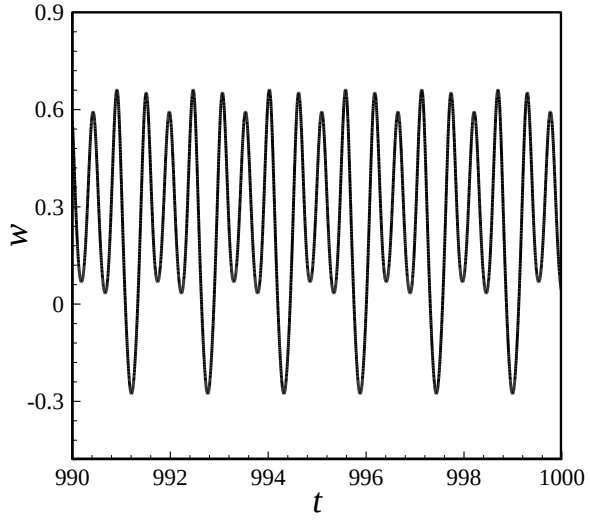
0.9
0.6
0.3
0
-0.3
w
990
992
994
996
998
1000
t

(b)

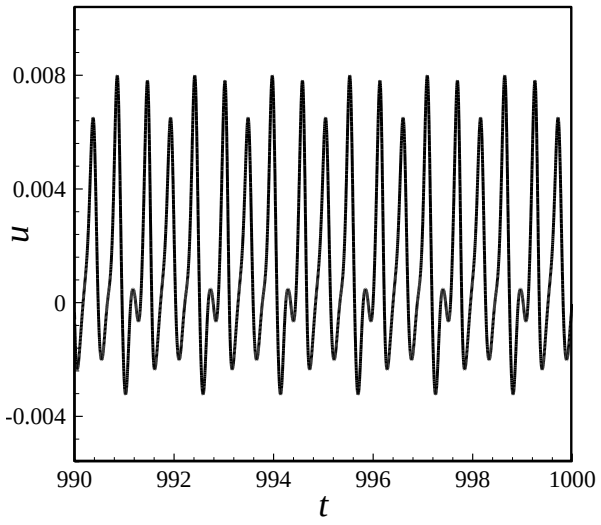
0.008
0.004
0
-0.004
u
990
992
994
996
998
1000
t

(c)

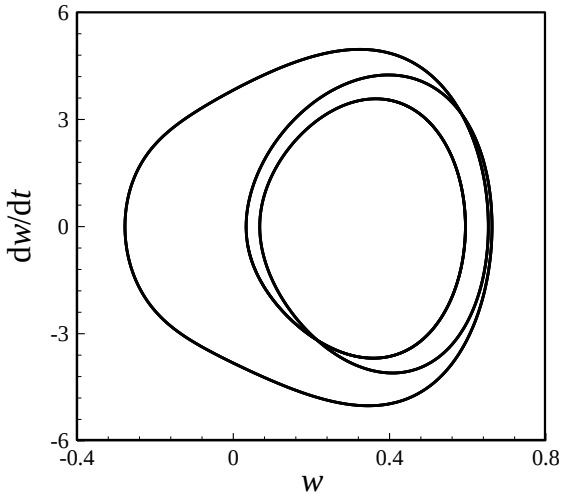
6
3
0
-3
-6
dw/dt
-0.4
0
0.4
0.8
w

(d)

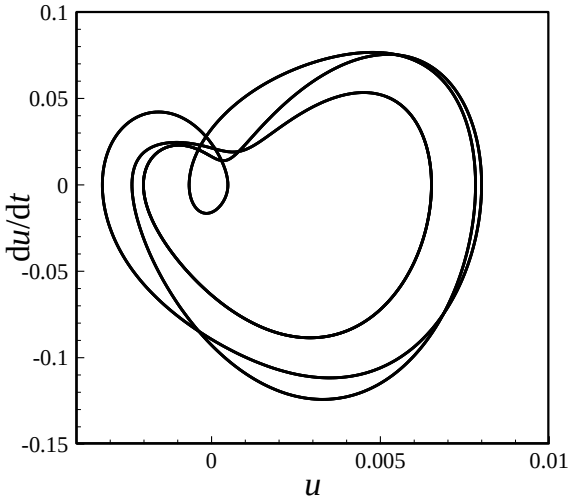
0.1
0.05
0
-0.05
-0.1
-0.15
du/dt
0
0.005
0.01
u

(e) (f)

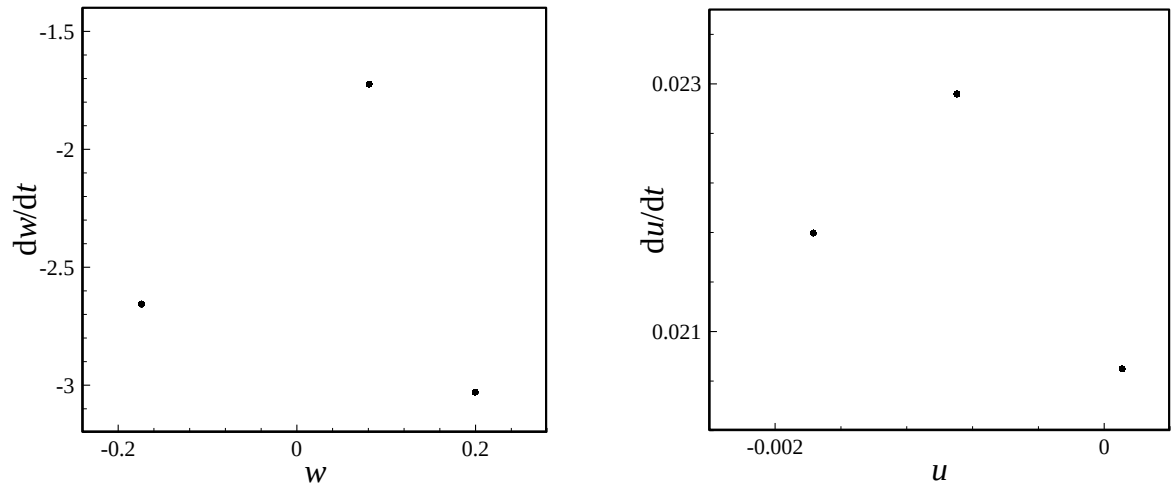

Figure 8: Dynamics of the nanosystem of Fig. 7 at F_1=26.0: (a, b) time histories of *w* (at *x*=0.5) and *u* (at *x*=0.65), respectively; (c, d) phase-plane portraits of *w* (at *x*=0.5) and *u* (at *x*=0.65), respectively; (e) Poincaré sections of *w* (at *x*=0.5) and *u* (at *x*=0.65), respectively.

(a)

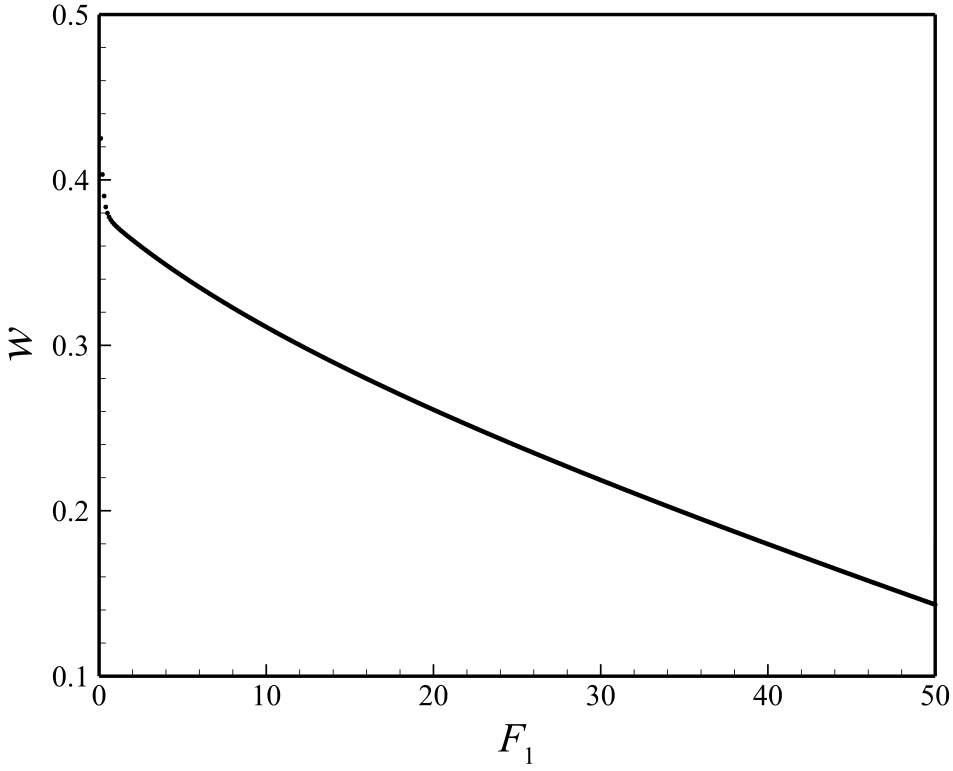

(b)

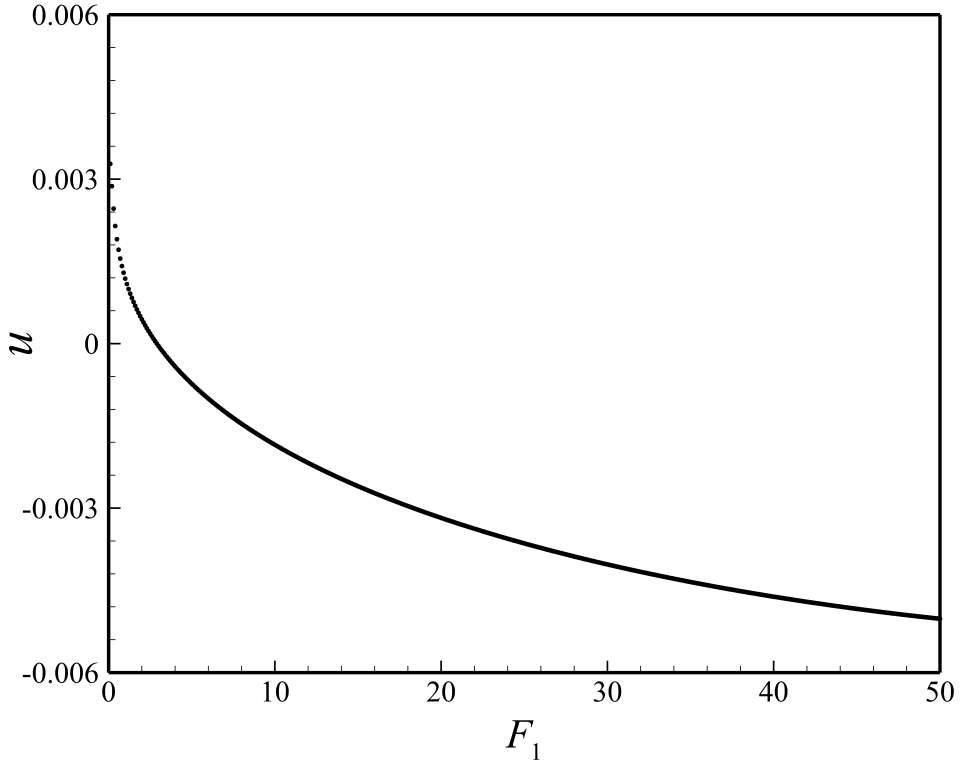

Figure 9: Bifurcation response of the initially imperfect viscoelastic tube conveying fluid flow at nanoscales: (a) *w* at *x*=0.50; (b) *u* at *x*=0.65 (*U* = 5.28, A_0=0.10, ω_1= 15.4546, and ω/ω_1=1.0).

(a)

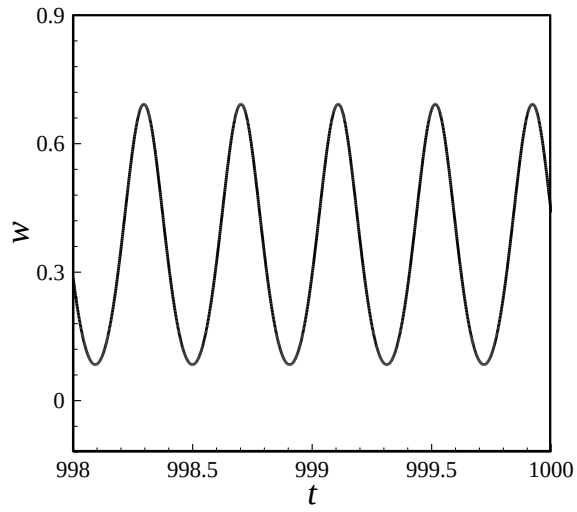
0.9
0.6
0.3
0
w
998
998.5
999
999.5
1000
t

(b)

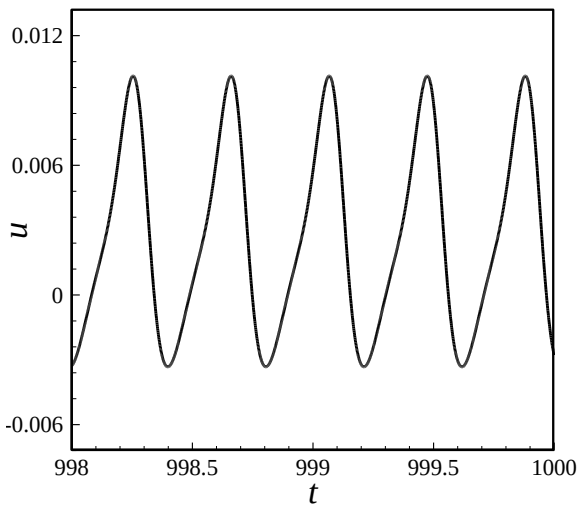
0.012
0.006
0
-0.006
u
998
998.5
999
999.5
1000
t

(c)

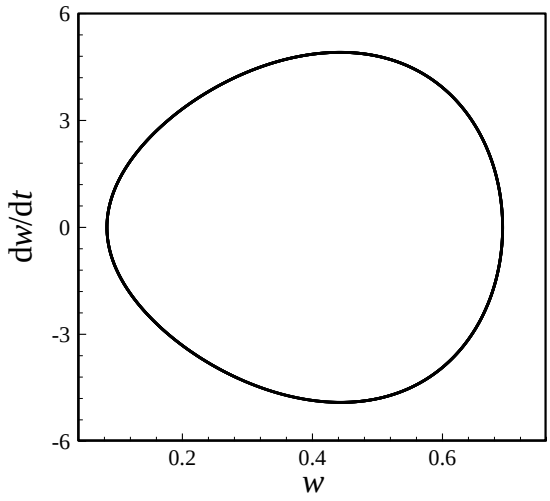
6
3
0
-3
-6
dw/dt
0.2
0.4
0.6
w

(d)

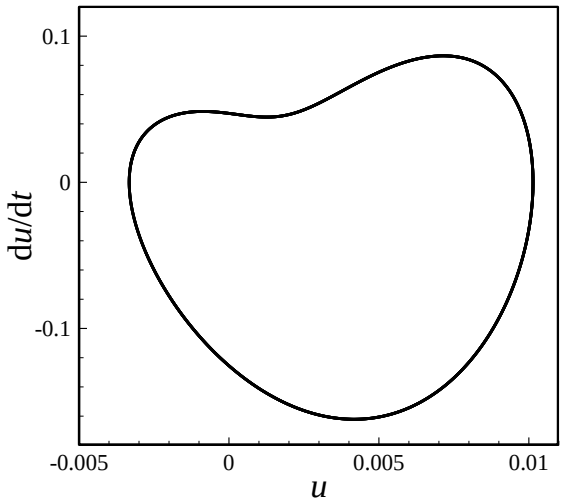
0.1
0
-0.1
du/dt
-0.005
0
0.005
0.01
u

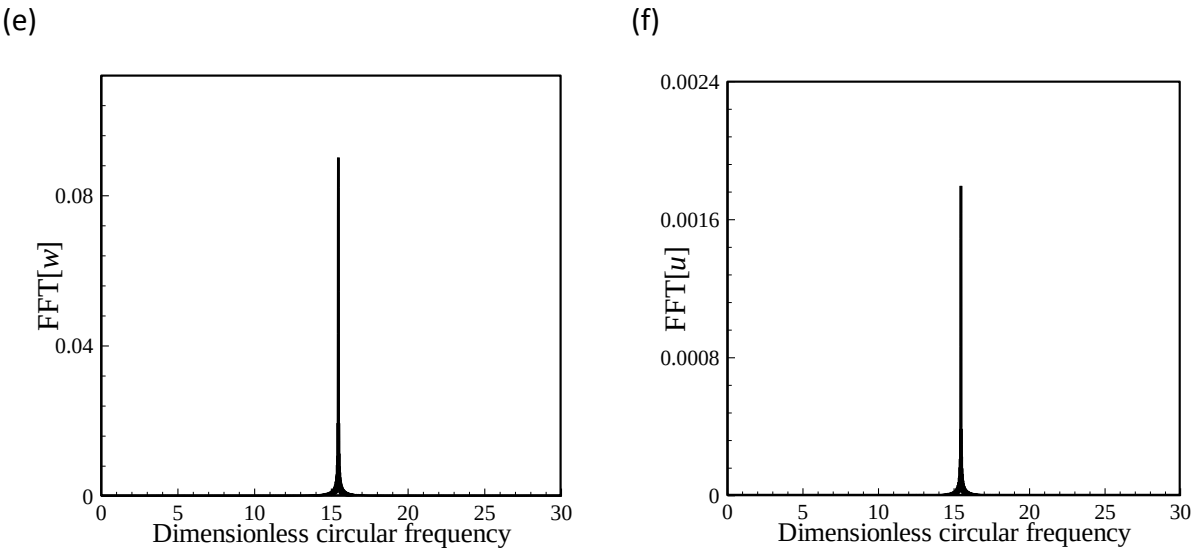

Figure 10: Dynamics of the nanosystem of Fig. 9 at F_1=20.0: (a, b) time histories of *w* (at *x*=0.5) and *u* (at *x*=0.65), respectively; (c, d) phase-plane portraits of *w* (at *x*=0.5) and *u* (at *x*=0.65), respectively; (e, f) FFTs of *w* (at *x*=0.5) and *u* (at *x*=0.65), respectively.

(a)

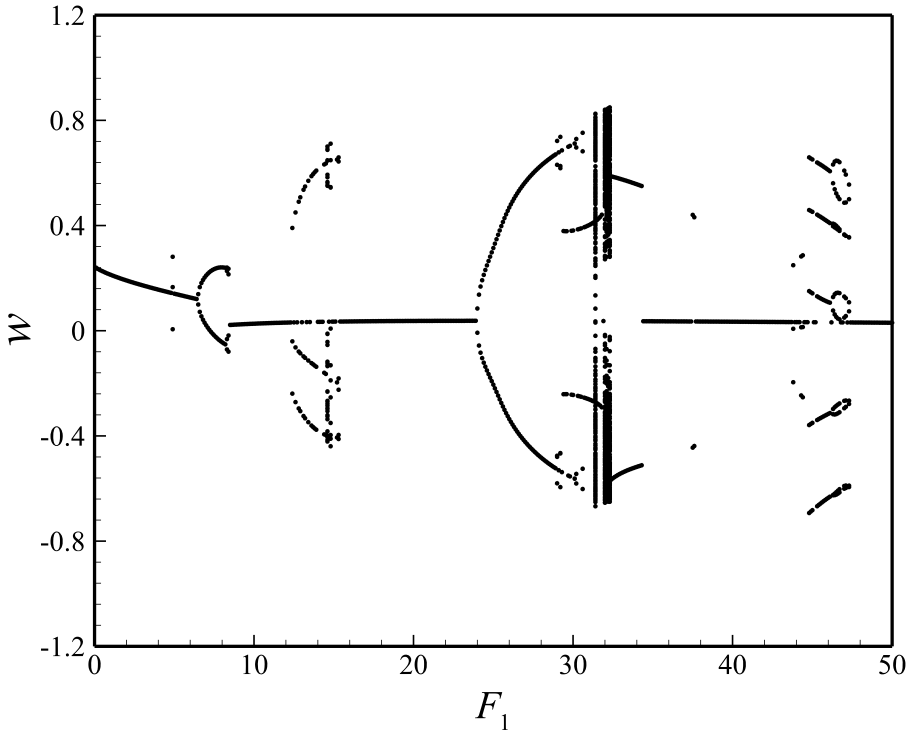

(b)

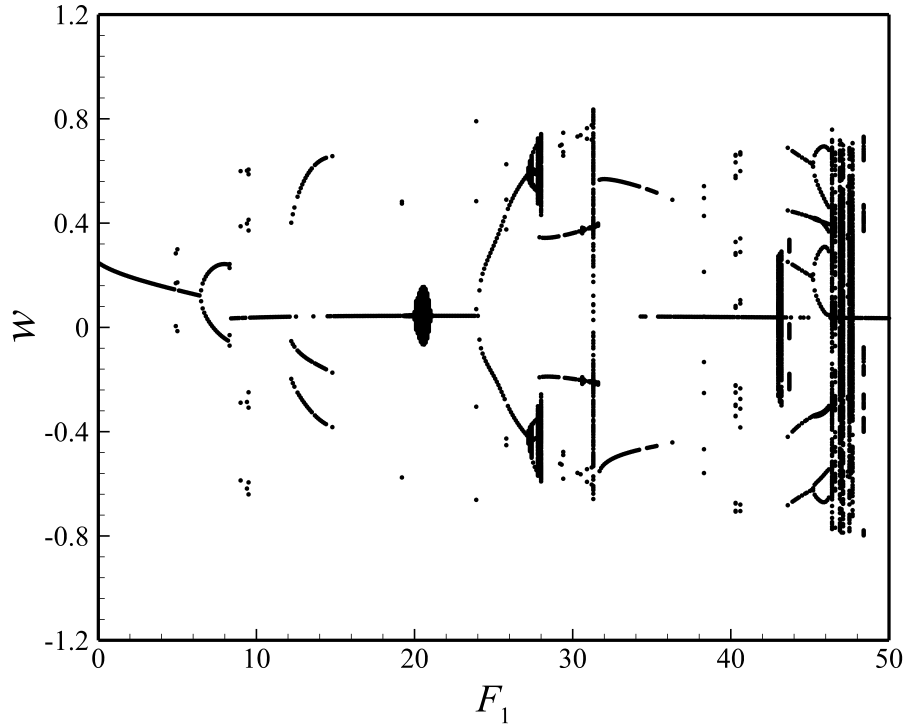

Figure 11: Comparison between bifurcation diagrams of Poincaré sections of the elastic and viscoelastic models of the initially imperfect tube conveying fluid flow at nanoscales: (a) w at x=0.50 based on the viscoelastic model; (b) w at x=0.50 based on the linear damping model (U = 5.28, A_0=0.01, ω_1= 7.1609, and ω/ω_1=1.0).